This is a preprint, the final version is subject to change, of the American Mineralogist (MSA)
Cite as Authors (Year) Title. American Mineralogist, in press.
(DOI will not work until issue is live.) DOI: http://dx.doi.org/10.2138/am-2017-5804

Revision 2

Controls on trace element partitioning among co-crystallizing minerals: Evidence from the Panzhihua layered intrusion, SW China

Lie-Meng Chen[1], Xie-Yan Song[1,*], Rui-Zhong Hu[1], Song-Yue Yu[1], Hai-Long He[1, 2], Yu-Wei She[1, 2], Zhi-Hui Dai[1] and Wei Xie[3]

[1] State Key Laboratory of Ore Deposit Geochemistry, Institute of Geochemistry, Chinese Academy of Sciences, Guiyang, 550081, P. R. China

[2] University of Chinese Academy of Sciences, Beijing, 100049, P. R. China

[3] State Key Laboratory of Isotope Geochemistry, Guangzhou Institute of Geochemistry, Chinese Academy of Sciences, Guangzhou, 510640, P. R. China

***Corresponding author: Xie-Yan Song**
Tel: 86 - 0851- 85895538
Fax: 86 - 0851- 85891664
Email: songxieyan@vip.gyig.ac.cn

This is a preprint, the final version is subject to change, of the American Mineralogist (MSA)
Cite as Authors (Year) Title. American Mineralogist, in press.
(DOI will not work until issue is live.) DOI: http://dx.doi.org/10.2138/am-2017-5804

ABSTRACT

The factors and processes that control trace element partitioning among co-crystallizing cumulus minerals in layered intrusions have long been controversial. Here we address this issue using new Laser Ablation ICP-MS trace element data for magnetite, ilmenite, and clinopyroxene from the Panzhihua layered intrusion in the Emeishan large igneous province, SW China. The cumulus minerals display strong Ni, Co, and Cr depletions, indicative of parental magmas low in concentration of these elements probably due to prior sulfide removal and the fractionation of chromite or Cr-magnetite in a staging magma chamber at depth. Both magnetite and clinopyroxene show cyclical variations in some transition elements (e.g., Cr, V, and Ni) up the stratigraphic section. The average concentrations of these transition elements in magnetite are positively correlated with those in clinopyroxene, likely resulting from co-crystallization of magnetite and clinopyroxene. The incompatible element (e.g., Zr, Hf, and Nb) concentrations of the cumulus minerals from the Lower Zone are highly variable compared to those of the Middle and Upper Zones. These large variations in trace element compositions are attributed to a “trapped liquid shift” in the Lower Zone. Ilmenite crystals from the Panzhihua intrusion may have undergone extensive modification of transition elements during subsolidus re-equilibration with magnetite, leading to the decoupled variations of transition elements in ilmenite across the Lower Zone stratigraphy. Our study indicates that systematic trace element variations of the main cumulus mineral assemblage, rather

than a single mineral, need to be considered to better constrain the magmatic differentiation and elemental fractionation of layered intrusions.

Keywords: Mineral trace element geochemistry; Fe-Ti oxides; Co-crystallization; Panzhihua layered intrusion; Emeishan Large Igneous Province

INTRODUCTION

Layered mafic intrusions provide important insights into magmatic fractionation and crystal accumulation processes in magma chambers (Wager and Brown 1967; Cawthorn 1996). Gravitational settling and dynamic sorting may result in the concentration of denser minerals (e.g., Fe-Ti oxides) in the cumulate rocks relative to lighter ones (e.g., plagioclase), giving rise to different mineral assemblages at different stratigraphic positions in the layered intrusions (Zhang et al. 2012; Maier et al. 2013; Song et al. 2013; Forien et al. 2015). Afterwards, compositions of cumulus minerals may be modified by trapped liquids and/or post-cumulus processes (Barnes 1986; Godel et al. 2011; Tanner et al. 2014). Thus, it is problematic to quantify the compositional differentiation of silicate magmas and partitioning of trace elements among co-crystallizing minerals (e.g., Tribuzio et al. 1999; Jang and Naslund 2001; Cawthorn 2007; Jourdan et al. 2007; Jakobsen et al. 2010). Long-standing issues regarding the petrogenesis of layered intrusions, e.g., the nature and evolution of the parental magmas in the Sept Iles layered intrusion (Namur et al. 2010) and the Bushveld Complex (Maier et al. 2013; Tanner et al. 2014), are still hot debated.

Recently, Laser Ablation Inductively Coupled Plasma Mass Spectrometry

(LA-ICP-MS) has made it possible to accurately determine in situ the trace element concentration of small volumes of cumulus minerals (e.g., Liu et al. 2008; Dare et al. 2012). LA-ICP-MS data have been used to elucidate igneous processes including fractional crystallization (Arndt et al. 2005; Godel et al. 2011; Dare et al. 2014; Liu et al. 2015), magma replenishment and mixing (Vantongeren and Mathez 2013; Luan et al. 2014; She et al. 2014, 2015), reactions between cumulate minerals and intercumulus liquid (Cawthorn 2013; Egorova and Latypov 2013; Tanner et al. 2014). However, the critical factors controlling the partitioning of trace elements among cumulus minerals are yet to be well constrained in layered intrusions, and are the focus of this study.

The Permian Panzhihua layered intrusion is a representative mafic-ultramafic igneous complex in the central part of the Emeishan Large Igneous Province (ELIP), SW China. Unusually thick, stratiform massive Fe-Ti oxides (up to 60 meter) and magnetite gabbro layers occur in its lower section (Panxi Geological Unit 1984). Although numerous studies were conducted on the origin of the Panzhihua Fe-Ti oxide orebodies (e.g., Zhou et al. 2005; Zhang et al. 2007; Ganino et al. 2008; Pang et al. 2008a, 2008b, 2009; Howarth and Prevec 2013; Song et al. 2013; Xing et al. 2014), the fundamental magmatic processes, including magmatic fractionation at depth, co-crystallization of cumulus minerals, and trapped liquid effects, are still poorly understood. In this work, we report a detailed study of trace element geochemical variations within magnetite, ilmenite, and clinopyroxene for the Panzhihua intrusion and discuss their implications for magmatic processes and petrogenesis of the

Panzhihua massive Fe-Ti oxides, magnetite gabbros, and gabbros.

GEOLOGICAL BACKGROUND

The ELIP is located in the southwestern part of the Yangtze Block, SW China, which consists of a Mesoproterozoic basement overlain by Neoproterozoic to Cenozoic sedimentary cover (Fig. 1a; Zhou et al. 2002). The ELIP contains mainly the Emeishan continental flood basalts, with minor picrite, tephrite and basaltic andesite, and the genetically related mafic-ultramafic layered intrusions and alkaline felsic plutons (Fig. 1b; Song et al. 2001, 2008; Xu et al. 2001, 2004; Ali et al. 2005; Zhang et al. 2006). The ELIP is believed to have formed from the end of the Guadalupian (~260 Ma) mantle plume (Chung and Jahn 1995; Song et al. 2001, 2004; Zhou et al. 2002).

Several mafic-ultramafic layered intrusions hosting giant Fe-Ti-V oxide deposits, including the Panzhihua, Hongge, Taihe and Baima layered intrusion, occur in the central part of the ELIP along the N-S trending Panzhihua- and Anninghe faults (Fig. 1b; Panxi Geological Unit, 1984; Zhang et al. 1988). SHRIMP zircon U-Pb age dating indicates that these intrusions formed between ~259 – 263 Ma (Zhou et al. 2002, 2008; Zhong and Zhu 2006; Zhong et al. 2011; Shellnutt et al. 2012; She et al. 2014). These layered intrusions are remarkable because they exhibit clear cyclical variations in mineral abundances, with mafic silicates + Fe-Ti oxides decreasing upward and plagioclase increasing upward. The Panzhihua and Baima intrusions are dominated by magnetite- and apatite-bearing gabbros or troctolite (Zhou et al. 2005; Pang et al.

2008a, 2008b; Zhang et al. 2012; Song et al. 2013; Liu et al. 2014), and the Hongge and Taihe intrusions contain olivine-clinopyroxenite and gabbro (Zhong et al. 2002; Bai et al. 2012, 2016; Luan et al. 2014; She et al. 2014). Thick stratiform Fe-Ti oxide layers are hosted in the lower and/or middle zones of these intrusions (Panxi Geological Unit, 1984).

GEOLOGY AND PETROGRAPHY

The Panzhihua layered intrusion (263 ± 3 Ma, Zhou et al. 2005) is a sill-like body (~19 km long and ~0.1 – 2 km thick, with an outcrop area of ~30 km^2) that strikes NE–SW and dips 40 – 60° to northwest. It is an elongated body that intruded into the Upper Neoproterozoic dolomitic limestone, schist, and gneiss. Apatite gabbro in Upper Zone is in faulted contact with Permian syenites and Triassic shales and coal formations (Fig. 1c; Panxi Geological Unit 1984). The intrusion has been divided into seven segments by a series of N-S-trending strike-slip faults as shown in Fig. 1c (Song et al. 2013).

The Panzhihua intrusion can be divided according to mineral assemblage and rock texture into a Marginal Zone at the base, overlain by a Lower Zone, Middle Zone and Upper Zone (Table 1; Fig. 1c). These divisions are after Song et al (2013) and Panxi Geological Unit (1984), and correspond to the Marginal Zone, Lower Zone, Middle Zone (a) and Middle Zone (b) of Pang et al (2008b), respectively. The Marginal Zone is dominated by microgabbro, which is mainly composed of fine-grained clinopyroxene and plagioclase with minor hornblende, magnetite,

ilmenite and olivine (Zhou et al. 2005).

Lower Zone

The Lower Zone is further subdivided into five cyclic units, from Unit I to V with decreasing Fe-Ti oxide content from the base to the top of each unit (Song et al. 2013). Unit I consists of coarse-grained magnetite gabbro and gabbro. Units II to V are characterized by thick massive Fe-Ti oxide layers (~40 – 60 meters) overlain by medium-grained magnetite gabbros and/or gabbros. Thin layers of magnetite gabbro also occur within the massive Fe-Ti oxide ore layers (Fig. 2a). The massive Fe-Ti oxide ore layers are marked by high Fe-Ti oxide contents (> 50 modal% magnetite and 10% ilmenite; the modal abundances of minerals were qualitatively estimated in thin section by Song et al. 2013) and low silicate abundance (< 40%, clinopyroxene + plagioclase ± olivine) and 1 – 4% sulfide contents (pyrrhotite and chalcopyrite, with minor pentlandite, Fig. 2b). The magnetite gabbros contain low abundances of cumulus Fe-Ti oxides (30 – 45% magnetite and 5 – 10% ilmenite) but high silicate contents (20 – 30% clinopyroxene, < 20 – 30% plagioclase, with minor olivine and hornblende), together with 1 – 3% sulfide (Fig. 2c-d). In the massive oxide layers and magnetite gabbros, most of the ilmenite crystals are in contact with magnetite, whereas in some magnetite gabbros a few ilmenite crystals are separated from magnetite by silicates. Contacts between magnetite and ilmenite are straight to slightly curved and commonly show ~120° triple junctions (Fig. 2b). Some plagioclase crystals show ductile deformed (bent) twins and have thin rims of brown hornblende (Fig. 2c-d). Most clinopyroxene crystals contain small and lineated platy

Fe–Ti oxides inclusions (Fig. 2 c-d), and a few clinopyroxene grains display clear overgrowth rims and anhedral hornblende rims (Fig. 2d). At the top of these cyclic units, the gabbros are distinguished by the lowest contents of interstitial Fe-Ti oxides (< 30%), and the highest contents of plagioclase (~30 – 45%) and clinopyroxene (~30 – 40%). Furthermore, the magnetite/ilmenite (Mt/Ilm) ratios of this zone generally decrease from the base (4.6 – 9.3) to the top (3.0 – 4.4) for each cyclic unit.

Middle Zone

The Middle Zone is subdivided into six cyclic units from VI to XI upward based on lithological variations (Song et al. 2013). Each cyclic unit is marked by magnetite gabbro at the base, and gabbro at the top with decreasing Fe-Ti oxide content. The magnetite gabbros in these cyclic units have lower Fe-Ti oxides (~30 – 45%) and higher plagioclase (~25 – 40%) contents than those of the Lower Zone (Fig. 2e). The mineral assemblage of the Middle Zone gabbro is identical to that of the Lower Zone, containing 20 – 35% Fe-Ti oxides, 30 – 45% plagioclase, and 25 – 40% clinopyroxene. Subhedral to euhedral magnetite and ilmenite grains are mainly separated by silicate minerals. The magnetite gabbros and gabbros in the Middle Zone are generally lower in Mt/Ilm ratios (1.5 – 4) than those in the Lower Zone (Mt/Ilm = 3.0 – 9.3). Compared to silicates in the Lower Zone, most clinopyroxene and plagioclase in the Middle Zone magnetite gabbros, and gabbros display more regular and linear edges with rare overgrowth rims or anhedral hornblende rims (Fig. 2e).

Upper Zone

The Upper Zone is characterized by the abrupt appearance of apatite gabbro, which contains <10% Fe-Ti oxides (rarely up to 15%), 50 – 65% plagioclase, 20 – 35% clinopyroxene, and ~3 – 5% apatite (Fig. 2f). Apatite occurs as small euhedral hexagonal crystals enclosed within plagioclase and clinopyroxene, or euhedral to subhedral grains intergrown among silicates and Fe-Ti oxides (Fig. 2f). Subhedral to euhedral magnetite and ilmenite grains are sparse usually separated by silicates. Furthermore, the Upper Zone rocks contain lower Mt/Ilm values (0.8 – 3) than the magnetite gabbros and gabbros in the Lower and Middle Zones (Pang et al. 2008a; Howarth et al. 2013; Song et al. 2013).

SAMPLING AND ANALYTICAL METHODS

Fifty-two samples across the whole lithostratigraphic section (except the Marginal Zone) were collected from the Zhujiabaobao open-pit mine, where the Lower and Middle Zones are the thickest and most well exposed (Fig. 1c). Polished thin sections of these rocks were prepared for *in situ* elemental analyses.

Major and trace element abundances of magnetite, ilmenite and clinopyroxene were determined *in situ* by LA-ICP-MS at the State Key Laboratory of Ore Deposit Geochemistry, Institute of Geochemistry, Chinese Academy of Sciences, using an Agilent 7700cs quadrupole ICP-MS coupled to a GeoLasPro 193 nm laser ablation system. The operating conditions and procedures were described in detail by Dare et al. (2012) and Liu et al. (2008) and are summarized as follows: laser beam diameter: 60 μm (for Fe-Ti oxides, BC-28, and GSE-1G) or 44 μm (for clinopyroxene,

193 BHVO-2G, NIST610, BIR-1G, and BCR-2G); laser pulse rate: 6 Hz; laser beam
194 fluence: ~10 J/cm^2 at the sample. Pure He was used as the carrier gas to pass the
195 ablation point within the cell, and mixed with Ar for improving efficiency for aerosol
196 transport. The total acquisition time for each analysis was 90 seconds (s), including
197 30s blank measurement (laser off) and 60s analysis (laser on). In this study, only the
198 cores of cumulus minerals were ablated and analyzed. Both fine-grained exsolution
199 lamellae (e.g., ilmenite, spinel, and magnetite) and the mineral host (e.g., magnetite,
200 ilmenite, and clinopyroxene) were ablated because the diameter of the laser beam (44
201 or 60 μm) is larger than the width of the exsolution lamellaes (< 20 μm, mostly < 10
202 μm). Therefore, the analytical results represent the initial compositions of magnetite,
203 ilmenite and clinopyroxene prior to subsolidus exsolution (Dare et al. 2012).
204 International reference standards GSE-1G and NIST610 were analyzed after
205 every eight analyses for Fe-Ti oxides and clinopyroxene, respectively, to monitor drift
206 in sensitivities. The in-house magnetite standard BC-28 (a massive magnetite from the
207 Bushveld complex, Barnes et al. 2004; Dare et al. 2012, 2014) and international
208 reference materials KL2-G and ML3B-G were measured as unknowns to monitor the
209 data quality of Fe-Ti oxides and clinopyroxene, respectively. Data reduction of Fe–Ti
210 oxides was conducted with the software *Igor-pro* (http://www.wavemetrics.com)
211 using Fe as the internal standard (see the Fe contents of magnetite in Song et al. 2013
212 and ilmenite in Zheng et al. 2014 as determined by electron microprobe). Data
213 reduction of clinopyroxene was performed with ICPMSDataCal using BHVO-2G,
214 NIST610, BIR-1G, and BCR-2G as external standards without internal

standardization (Liu et al. 2008), because clinopyroxene often hosts small Fe–Ti oxides inclusions as mentioned above. Detection limits for the Fe-Ti oxides and clinopyroxene were 0.1 – 4.4 ppm and 0.01 – 1 ppm, respectively. Analytical results of BC-28, KL2-G, and ML3B-G are consistent with their preferred values (Fig. 3, Table S1). Major and trace elements geochemical data of the Panzhihua magnetite, ilmenite and clinopyroxene are given in Table S2, S3 and S4, respectively.

RESULTS

Stratigraphic variations

Stratigraphic variations of several selected trace elements and MgO (or $Mg^{\#}$, where $Mg^{\#}$ = 100*MgO/[MgO + $FeO_{(T)}$, molar]) in magnetite, ilmenite, and clinopyroxene are illustrated in Fig. 4.

The variations in transition metal contents (e.g., Cr, V, Ni, and Sc) in the Lower Zone (Fig. 4) show that the average Cr and Ni contents of magnetite decrease upward in several cyclic units. For example, in Unit V, Cr varies from 490 ppm to 35 ppm, and Ni from 47 ppm to 19 ppm. Similarly, V and Sc concentrations in magnetite decrease upwards in each of these cyclic units. The magnetite within Unit I has the lowest Cr (7.2 – 10.1 ppm) and Ni (9.1 – 12.3 ppm) contents than any of the other units. Stratigraphic variations of Cr, Ni, V, and Sc in clinopyroxene are similar to those in magnetite. Average Ni and Sc contents in ilmenite decrease upward, but the variations of Cr and V in ilmenite display no clear trends (Fig. 4). It is noteworthy that the High Field Strength Element (HFSE, e.g., Zr, Hf, Nb, and Ta) and Rare Earth

Element (REE, e.g., La) concentrations in the Fe-Ti oxides and clinopyroxene in the Lower Zone are more variable than those in the Middle and Upper Zones (Fig. 4). Magnetite and clinopyroxene crystals in contact with anhedral hornblende have higher HFSE and REE than those not in contact with anhedral hornblende (Fig. 4, Tables S2, S4). In addition, ilmenite in contact with silicates in the magnetite gabbros contains higher Cr, V, and Co than those in contact with magnetite (Table S3). Both magnetite and ilmenite contain variable MgO contents from 0.82 to 3.68 wt% and from 2.95 to 7.25 wt%, respectively, while clinopyroxene has a small range of $Mg^{\#}$ values (72.0 – 79.4%, Fig. 4).

Magnetite and clinopyroxene in the Middle Zone show more regular changes and smaller cyclic variations in trace element concentrations than those in the Lower Zone (Fig. 4). Transition metals in magnetite and clinopyroxene decrease up stratigraphy in the Middle Zone. Both the magnetite and the clinopyroxene in the Middle Zone contain not only lower abundances of compatible elements (e.g., V and Cr), but also slightly lower incompatible element contents (e.g., Zr and La) than those in the Lower Zone (Fig. 4). Ilmenite in the Middle Zone has smaller variations in both major and trace element concentrations, and has slightly higher V contents than that in the Lower Zone (Fig. 4). In addition, magnetite and ilmenite in the Middle Zone have lower in MgO than those in the Lower Zone, decreasing up the stratigraphic column from 1.93 to 0.20 wt% and from 4.56 to 1.00 wt%, respectively (Fig. 4). Clinopyroxene in the Middle Zone has slightly lower $Mg^{\#}$ (70.3 – 74.6%) than that in the Lower Zone (Fig. 4).

In the Upper Zone, the Fe-Ti oxides and clinopyroxene are characterized by relatively small stratigraphic variations in most trace element and MgO (or $Mg^{\#}$) concentrations (Fig. 4). Both magnetite and clinopyroxene crystals from the Upper Zone contain significantly lower contents of transition metal contents (e.g., Cr, V, Ni, and Sc) than from the Lower and Middle Zones (Fig. 4). By contrast, the abundances of HFSE and REE, such as Zr and La, in the magnetite and clinopyroxene crystals of this zone are generally comparable to those of the Middle Zone, but lower than those of the Lower Zone (Fig. 4).

Multi-element variation patterns

Multi-element spider diagrams are used to compare the full suite of elemental concentrations in the Fe-Ti oxides and clinopyroxene (Figs, 5–7). Both trace and major elements from the Panzhihua magnetite are normalized to the Emeishan high-Ti picrite that was proposed to be compositionally similar to the primary magmas of the layered intrusions (Kamenetsky et al. 2012; Hou et al. 2013; Song et al. 2013) and are plotted in order of increasing compatibility with magnetite (Dare et al. 2012, 2014) (Fig. 5). The magnetite shows strong negative Ni, Co, Mg, and Sc anomalies and V, Zn, and Ga enrichments (Fig. 5). The trace element patterns of the Panzhihua magnetite resemble the basal magnetite of the Upper Zone magnetite layers in the Bushveld Complex (Dare et al. 2014), except the latter is relatively enriched in Sc, V, Ni, and Cr (Fig. 5). In addition, the Panzhihua magnetite becomes increasingly depleted in Ni, Cr, Co, Mg, and Sc from the Lower Zone massive Fe-Ti oxide layers, through the Lower and Middle Zone magnetite gabbros and gabbros to the Upper

Zone apatite gabbro (Fig. 5).

Eleven trace elements and four major elements of ilmenite are plotted in order of increasing compatibility (Jang and Naslund 2003; van Kan Parker et al. 2011; Dygert 2013) (Fig. 6). When normalized to the Emeishan high-Ti picrite (Kamenetsky et al. 2012), the Panzhihua ilmenite has similar patterns with significant Al, Ga, Co, Ni, Mg, and Cr depletions and slight Mn, V, and Ti enrichments (Fig. 6). Geochemical variations of the transition elements (e.g., V, Co, and Ni) in all ilmenite crystals are very small, whereas variations of Nb (= 27.3 – 79.5 ppm) and Hf (= 1.5 – 6.7 ppm) are large (Fig. 6).

The Panzhihua clinopyroxene trace element patterns normalized to the average composition of clinopyroxene phenocrysts in the Emeishan high-Ti picrite (Kamenetsky et al. 2012) are plotted in the order of increasing compatibility (Dygert et al. 2014). The clinopyroxene trace element patterns are generally flat with negative Ti, V, and Sc anomalies (Fig. 7). These negative anomalies become more distinct from the Lower Zone massive Fe-Ti oxide layers, through the Lower and Middle Zone magnetite gabbros and gabbros to the Upper Zone apatite gabbro. Except for the clinopyroxene in the Lower Zone Fe-Ti massive oxide layers, most clinopyroxene in the magnetite gabbros and gabbros and apatite gabbro are weakly depleted in Nb and Hf (Fig. 7).

DISCUSSION

The trace element concentrations in cumulus minerals depend primarily on the

following factors: (a) composition of the parental magmas, (b) fractional crystallization, and (c) their partition coefficients (Dare et al. 2014 and references therein). Furthermore, their compositions may also be modified by trapped intercumulus liquids (Barnes 1986; Godel et al. 2011) and/or diffusive interchange between adjacent crystals or fluids (e.g., Tanner et al. 2014). As mentioned above, the Panzhihua Lower and Middle Zones are dominated by massive Fe-Ti oxide ores, magnetite gabbros, and gabbros, which are composed of magnetite, ilmenite, clinopyroxene, plagioclase, and minor olivine, whereas the Upper Zone apatite gabbro is rich in cumulus apatite. Song et al. (2013) proposed that the Panzhihua magnetite and ilmenite co-crystallized with clinopyroxene, after the crystallization of olivine and plagioclase. In the following sections, we discuss the main processes and factors that control the partitioning of trace elements into the Panzhihua Fe-Ti oxides and clinopyroxene based on the concentrations and correlations of these minerals.

Prior fractionation and sulfide removal at depth

The relatively low forsterite (Fo) values of all olivine crystals (< 82.5 mol%) suggest that the Panzhihua parental magma was moderately evolved prior to emplacement (Pang et al. 2009; Zhang et al. 2011). Moreover, the Panzhihua cumulate rocks are characterized by high Cu/Ni and Pd/Ir ratios (Zhou et al. 2005; Howarth and Prevec 2013). MELTS thermodynamic calculations (Ghiorso and Sack 1995) indicate that the Panzhihua parental magma was generated after fractionating spinel, olivine, and clinopyroxene from a picritic magma in a deep-seated magma chamber (Song et al. 2013). These results demonstrate that the Panzhihua parental

magma may have undergone fractionation prior to emplacement. This is further supported by the Panzhihua clinopyroxene compositions, because these minerals (especially those from the Lower Zone rocks) contain higher HFSE and REE than clinopyroxene from the Emeishan high-Ti picrite (Fig. 7a). This implies that the parental magma entering the Panzhihua magma chamber was indeed moderately evolved, as it was more enriched in incompatible elements (i.e. HFSE and REE) than the Emeishan high-Ti picrite.

In the normalized multi-element diagrams, the Panzhihua magnetite and ilmenite display strongly negative Ni and Co anomalies (Figs. 5, 6). Both Ni and Co are compatible in magnetite and ilmenite (see partition coefficients in Table S5). A potential interpretation for these negative anomalies is *in situ* sulfide liquid immiscibility along with crystallization of Fe-Ti oxides in the Panzhihua magma chamber, because Ni and Co partition strongly into immiscible sulfide liquids ($D_{Ni}^{Sul/Liq}$ = 500 – 800, Peach et al. 1990, $D_{Co}^{Sul/Liq}$ = 61 – 80, Rajamani and Naldrett 1978). However, the high modal of primary sulfide (up to ~4%, pyrrhotite and chalcopyrite, with minor pentlandite; Song et al. 2013), and low Ni contents (< 100 ppm) of the Panzhihua cumulate rocks (Zhou et al. 2005; Howarth and Prevec 2013) suggest a weak contribution from *in situ* sulfide immiscibility on the Ni and Co depletions in magnetite and ilmenite.

Alternatively, these negative anomalies may result from Ni and Co depletions in the Panzhihua parental magma. These depletions could be attributed to olivine fractionation ($D_{Ni}^{Ol/Liq}$ = 22.3 ± 9.12, $D_{Co}^{Ol/Liq}$ = 5.2 ± 1.5, Laubier et al. 2014) and/or

345 removal of sulfide liquids at depth. However, MELTS simulations indicated that
346 proportions of crystallized olivine were relatively low (~2.4 wt%) prior to
347 emplacement (Song et al. 2013), and thus olivine fractionation alone could not be
348 responsible for the observed Ni and Co depletions in magnetite and ilmenite.
349 Consequently, Ni and Co depletions of the parental magma are attributed to sulfide
350 segregation and removal at depth. This hypothesis is evidenced by the depletion of
351 platinum group elements and very high Cu/Pd values (> 60,000) of the Panzhihua
352 rocks relative to the genetically related Emeishan high-Ti basalts (Howarth and
353 Prevec 2013). In addition, the magnetite and ilmenite in the Middle and Upper Zones
354 are progressively more depleted in Ni and Co than those in the Lower Zone (Figs. 5,
355 6), indicating a coupling of sulfide segregation and Fe-Ti oxide crystallization in the
356 Panzhihua magma chamber.

357 Although Cr is compatible in Fe-Ti oxides ($D_{Cr}^{Mt/Liq}$ = 19.3 – 340, Dare et al.
358 2014; $D_{Cr}^{Ilm/Liq}$ = 5.9 – 22.4, Dygert et al. 2013; Table S5), both magnetite and
359 ilmenite in the Panzhihua intrusion show strong negative Cr anomalies in the
360 multi-element normalized diagrams (Figs. 5, 6). In addition, magnetite from the
361 Lower Zone rocks contains much lower Cr (~10 – 450 ppm) than magnetite from the
362 megacyclic Unit I of the Sept Iles layered intrusion, Canada (Cr = 5600 – 12300 ppm,
363 Namur et al. 2010). On the other hand, the Panzhihua olivine and plagioclase are
364 slightly more primitive ($Fo_{54–82}$, $An_{40–70}$, Pang et al. 2009; Zhang et al. 2011) than
365 their Sept Iles counterparts ($Fo_{50–72}$, $An_{34–69}$, Namur et al. 2010), suggesting that the
366 Panzhihua parental magma was less evolved than that in the Sept Iles intrusion. The

significant Cr depletions in the Panzhihua magnetite and ilmenite cannot be ascribed to either silicate fractionation or sulfide removal, because Cr is moderately incompatible or compatible in silicates ($D_{Cr}^{Ol/Liq}$ = 0.63 – 1.85, Kloeck and Palme 1988; Beattie 1994; $D_{Cr}^{Cpx/Liq}$ = 1.66 – 3.8, Hart and Dunn 1993; Hauri et al. 1994; $D_{Cr}^{Plagioclase/Liq}$ = 0.019 – 0.365, Aignertorres et al. 2007) and sulfides ($D_{Cr}^{Sul/Liq}$ = 0.9, Pedersen 1979). The bulk partition coefficient of Cr would be slightly incompatible overall if only silicates crystallized. Instead, such depletions most likely reflect early chromite and/or Cr-magnetite fractionation, which would have scavenged Cr to generate the major Cr depletion seen the residual magma and thus in magnetite and ilmenite. The fine-grained chromite/or Cr-magnetite inclusions (Cr_2O_3 = 2.0 – 10.8 wt%) in olivine from the Lower Zone rocks were thought to be early crystallized and trapped Fe-Ti oxide crystals (Pang et al. 2008a) or xenocrysts (Howarth et al. 2013; Zhou et al. 2013), lending further support to the above interpretation.

Co-crystallization of Fe-Ti oxides and clinopyroxene

At the oxygen fugacity of the quartz-fayalite-magnetite buffer, saturation of Fe-Ti oxides generally occurs during the late stages of fractionation in mafic magmas (i.e. the Fenner trend; Fenner, 1929; Wager and Brown 1967; Frost and Lindsley 1991; Toplis and Carroll 1995; Thy et al. 2006). Therefore, Fe-Ti oxide rich layers commonly occur in the upper sections of layered intrusions, such as the Bushveld Complex, and the Skaergaard intrusion (Cawthorn and Molyneux 1986; Eales and Cawthorn 1996; Tegner et al. 2006). However, stratiform massive Fe-Ti oxide layers and magnetite gabbros occur in the Lower and Middle Zones at Panzhihua. This

389 feature is also the case for the Sept Iles layered intrusion, where 24 layers of massive
390 Fe-Ti oxide ore (up to 1 meter thick) occur in the troctolites of the Layered Series in
391 its lower section. The formation of the Sept Iles Fe-Ti oxide ore layers was attributed
392 to early Fe-Ti oxide saturation together with olivine and plagioclase crystallization
393 from a ferrobasaltic liquid (Namur et al. 2010). Compared to the Sept Iles intrusion,
394 the Panzhihua intrusion was formed from a relatively primitive parental magma, in
395 which magnetite and clinopyroxene crystallized after olivine and plagioclase (Song et
396 al. 2013). This co-crystallization suggests that magnetite, ilmenite, and clinopyroxene
397 could compete for the (more) compatible trace elements.

398 As mentioned above, the transition metals (e.g., Ni, Cr, and V) are compatible in
399 magnetite, ilmenite, and clinopyroxene (see partition coefficients in Table S5). The
400 strong decreases of Ni, Cr, and V contents in magnetite and clinopyroxene with
401 stratigraphic height within several Lower Zone cyclic units (Fig. 4) reflect a depletion
402 of these elements in the residual liquids in response to early magnetite and
403 clinopyroxene crystallization (i.e. $D_{bulk}^{Ni, Cr, V} > 1$). The repetitive reversals of Ni, Cr,
404 V, and MgO (or $Mg^{\#}$) contents in magnetite and clinopyroxene from the cyclic units
405 of the Panzhihua intrusion indicate multiple magma replenishments (Fig. 4). These
406 reversals are consistent with cyclic variations of chemostratigraphic columns of the
407 Panzhihua whole rocks (Song et al. 2013), and are also similar to the
408 chemostratigraphic variations of the Bushveld complex (Cawthorn 2007; Tanner et al.
409 2014). Moreover, the positive correlations of Ni, Cr, V, and Sc in the Panzhihua
410 magnetite and clinopyroxene imply that they co-crystallized from the parental magma

411 (Fig. 8a-d). The Sc concentrations in clinopyroxene from the Lower Zone are higher
412 than those in the Emeishan high-Ti picrite (Fig. 7), demonstrating that the Panzhihua
413 parental magma was not Sc depleted. The increasingly negative Sc anomalies in
414 magnetite from the Lower Zone to the Middle and Upper Zones (Fig. 5) suggest
415 co-crystallization of clinopyroxene and magnetite with increasing proportions of
416 clinopyroxene upward because Sc is preferentially partitioned into clinopyroxene (see
417 partition coefficients in Table S5, the D_{bulk} would be compatible for Sc according to
418 proportions of crystallized minerals proposed by Song et al. 2013). On the other hand,
419 Nb and Ta are compatible and Zr and Hf are moderately incompatible in ilmenite
420 (Dygert et al. 2013), while these elements are highly incompatible for olivine,
421 clinopyroxene, and plagioclase (see partition coefficients in Table S5). The flat
422 normalized multi-element patterns of the Lower Zone clinopyroxene suggest that
423 ilmenite crystallization may not have played a critical role in the partitioning of Nb,
424 Ta, Zr, and Hf into clinopyroxene (Fig. 7a). Magnetite and clinopyroxene (plagioclase
425 as well) were therefore likely major early cumulate phases that fractionated soon after
426 the parental magma entered the Panzhihua magma chamber. The ilmenite in the
427 Lower Zone, however, crystallized from the parental magma somewhat after
428 magnetite and clinopyroxene. Consequently, the Lower Zone magnetite gabbros have
429 lower TiO_2 than the Middle Zone magnetite gabbros with the same $Fe_2O_{3(T)}$ (Zhou et
430 al. 2005; Pang et al. 2008b; Song et al. 2013). Co-crystallization of magnetite and
431 clinopyroxene in this study is inconsistent with the proposed model, which argued
432 that the silicates were not in equilibrium with the Fe-Ti oxides and the massive ores

formed without the presence of silicates due to intrusion of H_2O-rich magma (Howarth et al. 2013).

The clinopyroxene in the Middle and Upper Zone rocks is more depleted in Nb, Zr, and Hf than that in the Lower Zone rocks (Fig. 7). These depletions indicate that ilmenite and clinopyroxene co-crystallized, and that the increasing proportion of ilmenite scavenges Nb, Zr, and Hf from the Lower Zone to the Middle and Upper Zones, given that these elements are preferentially partitioned in ilmenite (see partition coefficients in Table S5). This proposal also agrees with the observed decreases in Mt/Ilm ratios upward the section. The positive correlations of Sc and Zr between ilmenite and clinopyroxene from the Middle and Upper Zone rocks (especially gabbros) (Fig. 8d-e) demonstrate their co-crystallizing relationship. The scattered correlations in Cr and V contents between ilmenite and clinopyroxene (Fig. 8a-c) may indicate diffusive modification during subsolidus re-equilibration upon cooling (see discussion below). Furthermore, positive correlations of Ni, Cr, V, and Sc between magnetite and clinopyroxene in the Middle and Upper Zone rocks indicate not only a co-crystallizing relationship, but also a decrease of these elements in the residual magma after extensive magnetite, ilmenite, and clinopyroxene fractionation (Fig. 8a-d).

Trapped liquid shift in the Lower Zone

The concentrations of incompatible trace elements, particularly the highly incompatible Zr, Nb, and REE, in magnetite and clinopyroxene in the Lower Zone (and Unit VI in the Middle Zone) are higher than those in the Middle (Units VII–XI)

455 and Upper Zones (Fig. 4, Tables S2, S4). This is in contrast to the expected
456 geochemical variations, which would become more enriched up stratigraphy because
457 of their incompatible behavior (e.g., Dare et al. 2014). Moreover, the incompatible
458 element contents in different magnetite (as well as clinopyroxene) grains within a
459 single sample in the Lower Zone are highly heterogeneous compared to those in the
460 Middle and Upper Zones (Fig. 4, Tables S2, S4). These features are difficult to
461 explain through fractionation alone, and may result from subsequent elemental
462 modification during crystallization of the trapped intercumulus liquids (i.e. trapped
463 liquid shift, Barnes 1986).

464 The effects of trapped liquids have been widely documented in cumulates from
465 mafic-ultramafic layered intrusions and have been used to interpret mineral
466 compositions in cumulate rocks (e.g., Cawthorn 1996, 2007, 2013; Lundgaard, et al.
467 2006; Egorova and Latypov 2013). Song et al. (2013) estimated that the proportions
468 of trapped liquids in the Panzhihua Lower and Middle Zone rocks were below 5%
469 using whole-rock P concentrations. Similarly, Bai et al. (2014) proposed that less than
470 5% of trapped liquid existed in the Panzhihua massive Fe-Ti oxide layers based on
471 whole rock REE contents. The small percentages of trapped liquids in the Lower Zone
472 indicate that the porosity in these rocks was low, perhaps due to significant
473 compaction by the gravitational settling of Fe-Ti oxides and clinopyroxene during the
474 formation of this zone. This is supported by the ductile deformation (bent) of the
475 plagioclase crystals in the magnetite gabbro (Fig. 2c).

476 The magnitude of the trapped liquid shift on mineral compositions depends on

477 the amount of trapped liquid, the modal ratios of the cumulus phases, and the partition
478 coefficient for one element (Barnes 1986; Cawthorn 2007). Minor interstitial
479 clinopyroxene and plagioclase, together with hornblende rims around these minerals
480 (Fig. 2b-d) in the Lower Zone massive Fe-Ti oxide layers and magnetite gabbros,
481 suggest that the modal proportions of trapped liquid were quite low. The trapped
482 liquid would become increasingly enriched in incompatible trace elements with
483 decreasing temperature. Therefore, the incompatible trace element contents of the
484 magnetite and clinopyroxene in contact with intercumulus liquid would be
485 significantly modified by re-equilibration and/or overgrowth. This hypothesis is
486 supported by the observations that the magnetite and clinopyroxene with hornblende
487 rims have higher incompatible trace element contents than those not in contact with
488 hornblende rims (Fig. 4, Tables S2, S4). Such "trapped liquid shift" is also recorded
489 by the overgrowth rim of clinopyroxene (Fig. 2d). On the other hand, for the
490 compatible elements (such as Ni, Cr, V, and Sc), this shift could be trivial and ignored
491 in the Lower Zone, because these elements in the intercumulus liquid would be
492 buffered well by magnetite, ilmenite, and clinopyroxene (Cawthorn 2007).

493 By contrast, trace element abundances in Fe-Ti oxides and clinopyroxene from
494 individual samples within the upper part of Middle (Units VII–XI) and Upper Zones
495 are commonly homogeneous (Fig. 4; Tables S2, S4). This suggests that the role of
496 trapped liquids on the cumulus minerals in these rocks is insignificant. This
497 hypothesis can be further tested using Ni, Cr, and V contents in the cumulus minerals.
498 For the upper part of the Middle (Units VII–XI) and Upper Zone rocks, the gabbros

499 and apatite gabbros have high proportions of plagioclase (30 – 65%), in which Ni, Cr,
500 and V are highly incompatible. Since cumulus plagioclase cannot buffer Ni, Cr, and V
501 contents in the intercumulus liquids, the trapped liquid shift would result in much
502 lower concentrations of these elements in clinopyroxene and magnetite than what
503 would be produced during equilibrium crystallization (Cawthorn 2007; Tanner et al.
504 2014). This expectation is not observed in the stratigraphic variations of trace
505 elements, as magnetite and clinopyroxene do not display abrupt decreases of Ni, Cr,
506 and V contents from the magnetite gabbros to the gabbros and apatite gabbros (Fig. 4),
507 suggesting no extensive trapped liquid shift in these rocks. It was likely that most of
508 the residual liquids were squeezed out of the chamber during the formation of the
509 Middle and Upper Zones (Pang et al. 2009), as evidenced by the homogenous
510 clinopyroxene crystals without late stage overgrowth rims in these zone rocks (Fig.
511 2e).

512 **Diffusive modification of transition elements in ilmenite**

513 Unlike magnetite and clinopyroxene, the Panzhihua ilmenite unexpectedly shows
514 decoupled variations in transition elements (e.g., Cr and V) with stratigraphic height
515 in the Lower Zone (Fig. 4). It would be expected decrease upward, due to their
516 compatible behavior, in each cyclic unit. The correlation of Cr contents between
517 ilmenite and clinopyroxene in the Lower Zone is less defined than that between
518 magnetite and clinopyroxene, whereas Cr contents are positively correlated between
519 ilmenite and clinopyroxene in the Middle and Upper Zones (Fig. 8b). Similar
520 correlation of V contents between ilmenite and clinopyroxene is observed in these

zones (Fig. 8c). Such compositional variations in the Lower Zone ilmenite are difficult to explain by either prior fractionation at depth, co-crystallization, or trapped liquid shift as discussed above.

An alternative explanation for the decoupled variations of the ilmenite transition elements in the Lower Zone is diffusive modification of these elements between the Fe-Ti oxides during subsolidus re-equilibration. Previous studies have demonstrated that subsolidus re-equilibration involves the exchange of Fe^{3+}, Ti^{4+}, Fe^{2+}, and Mg^{2+} among Fe-Ti oxides (as well as silicates) in layered intrusions (Frost and Lindsley 1991; Pang et al. 2008b). The straight to slightly curved contacts between Panzhihua magnetite and ilmenite crystals indicate that they have undergone significant subsolidus re-equilibration (Fig. 2b). It is thus reasonable to infer that the trace elements may have been redistributed among the Fe-Ti oxides during subsolidus re-equilibration upon cooling. Such redistributions would be controlled by the relative partition coefficients for the different minerals (e.g., $K_{D(Cr, V)}^{Mt/Ilm}$, Tanner et al. 2014). With decreasing temperature, the transition elements diffused from ilmenite into magnetite in which they are more compatible (e.g., $K_{D(Cr, V)}^{Mt/Ilm} > 1$, Table S5). Meanwhile, the diffusive redistributions of the transition elements are affected by relative modal abundances of magnetite and ilmenite in the rocks according to the mass balance relation. In the Lower Zone, magnetite is a dominant mineral in the massive Fe-Ti oxide layers and magnetite gabbros. In these rocks, Cr and V diffusing into magnetite from ilmenite could not significantly modify the primary compositions of magnetite because of high modal abundances of magnetite relative to ilmenite

543 (Mt/Ilm = 3.0 – 9.3 in the Lower Zone). On the other hand, this diffusive
544 re-equilibration would result in distinct decreases in Cr and V in the ilmenite.
545 Consequently, the magnetite has seen large decreases of Cr and V in the Lower Zone
546 as expected from fractional crystallization, while the ilmenite shows low and constant
547 Cr and V contents in the massive Fe-Ti oxide layers, resulting in weak correlations
548 between magnetite and ilmenite (Fig. 9). These results are consistent with the
549 extensive Fe isotope exchange between magnetite and ilmenite documented in the
550 lower zone of the Baima layered intrusion in the ELIP. Chen et al (2014) suggested
551 that the magnetite preserved its original magmatic Fe isotope signatures (δ^{57}Fe = 0.15
552 – 0.36, in agreement with values of 0.20 – 0.36 that would be expected for minerals in
553 equilibrium with the parental magma) whereas the ilmenite compositions (δ^{57}Fe =
554 -0.82 – -0.30, much lower than the predicted values of -0.15 – -0.04) were modified
555 during subsolidus re-equilibration.

556 On the other hand, magnetite and ilmenite in the Middle and Upper Zones are
557 mainly in contact with silicate minerals (Fig. 2f), which were last equilibrated with
558 Fe-Ti oxides at ~950 °C (Pang et al. 2008b). Thus, redistributions of transition
559 elements between magnetite and ilmenite in the Middle and Upper Zone rocks would
560 not be very significant upon cooling compared to those in the massive Fe-Ti oxide
561 layers. Consequently, the transition elements display roughly positive correlations
562 between magnetite, ilmenite, and clinopyroxene in the Middle and Upper Zone rocks
563 with low proportions of Fe-Ti oxides (especially in the Upper Zone samples) (Figs. 8,
564 9). Furthermore, ilmenite in contact with magnetite in the magnetite gabbro of the

Lower Zone contains lower Cr and V than that in contact with silicates, giving additional support to the above interpretation (Table S3).

CONCLUSIONS AND IMPLICATIONS

Trace element variations among magnetite, ilmenite, and clinopyroxene from the Panzhihua layered intrusion are primarily controlled by magma compositions, co-crystallizing minerals, trapped liquid shift, and subsolidus re-equilibration. Prior removal of a sulfide liquid and the fractionation of chromite and/or Cr-magnetite at depth resulted in depletions of Ni, Co, and Cr in the parental magmas, and thus in the magnetite, ilmenite and clinopyroxene they produced. Fractional crystallization of olivine and clinopyroxene at deep levels also gave rise to the enrichment of incompatible trace elements in the parental magmas. In the Lower Zone, early co-crystallization of magnetite and clinopyroxene resulted in positive correlations in the transition metal contents (e.g., Ni, Cr, V, and Sc), while ilmenite crystallized somewhat after magnetite and clinopyroxene. In the Middle and Upper Zones, however, ilmenite crystallized concurrently with magnetite and clinopyroxene, which produced the negative Nb, Zr, Hf, and Ti anomalies in clinopyroxene. These results further support our proposed genetic model, in which the fractionation of silicates at depth and early Fe-Ti oxide saturation in the shallow magma chambers are key factors in the formation of the massive Fe-Ti oxides layers at Panzhihua (Zhang et al. 2011; Song et al. 2013; Zheng et al. 2014). The trapped intercumulus liquids may have significantly altered the original contents of incompatible trace elements (e.g., Zr, Nb,

and Hf) in magnetite, ilmenite, and clinopyroxene and caused the distinct elemental heterogeneity of these elements in all the Lower Zone cumulus minerals; while such effects were insignificant in the Middle and Upper Zones. This interpretation is further supported by the find that magnetite and clinopyroxene adjacent to hornblende rims have higher incompatible trace element contents than those not in contact with hornblende.

The reliability of using the elemental composition of any single cumulus mineral (e.g., clinopyroxene) and partition coefficients to back-calculate the parental magma composition of a layered intrusion is problematic, since the minerals may have been in competition for trace elements and/or experienced trapped liquid shift. Furthermore, we found that Fe-Ti oxides may have undergone extensive elemental re-equilibration by diffusion, which modified the original magmatic signature of the Lower Zone ilmenite. Thus, the critical processes controlling trace element partitioning in cumulate minerals should be investigated before applying magnetite trace element geochemistry as a petrogenetic indicator to discriminate ore deposit types and their formation settings and mechanisms.

ACKNOWLEDGEMENTS

This work was funded by CAS/SAFEA International Partnership Program for Creative Research Teams - (Intraplate Mineralization Research Team; KZZD-EW-TZ-20), the strategic priority research program (B) of the Chinese Academy of Sciences (XDB18030203), the NSFC (41473024, 41373042, and 41473050), and the National

607 Basic Research Program of China (2012CB416804). We acknowledge Sarah Dare and
608 Dominique Tanner for their constructive and detailed reviews, and Fidel Costa for his
609 suggestions and editorial handling. Special thanks are given to Dany Savard for
610 providing the in-house standard magnetite BC-28 and geochemical calibration.
611 Fang-Zhen Teng, Aaron Brewer, and Cenozoic Geoscience Editing & Consultancy are
612 thanked for polishing language.

613 **REFERENCES CITED**

614 Aignertorres, M., Blundy, J., Ulmer, P. and Pettke, T. (2007). Laser ablation ICPMS
615 study of trace element partitioning between plagioclase and basaltic melts: an
616 experimental approach. Contributions to Mineralogy and Petrology, 153, 647–
617 667.
618 Ali, J.R., Thompson, G.M., Zhou, M.-F., and Song, X.-Y (2005) Emeishan large
619 igneous province, SW China. Lithos, 79, 475–489.
620 Arndt, N., Jenner, G., Ohnenstetter, M., Deloule, E., and Wilson, A. (2005) Trace
621 elements in the Merensky Reef and adjacent norites Bushveld Complex South
622 Africa. Mineralium Deposita, 40, 550–575.
623 Bai, Z.-J., Zhong, H., Naldrett, A.J., Zhu, W.-G., and Xu, G.-W. (2012) Whole-Rock
624 and Mineral Composition Constraints on the Genesis of the Giant Hongge Fe–
625 Ti–V Oxide Deposit in the Emeishan Large Igneous Province, Southwest China.
626 Economic Geology, 107, 507–524.
627 Bai, Z.-J., Zhong, H., Li, C., Zhu, W.-G., He, D.-F., and Qi, L. (2014) Contrasting

parental magma compositions for the Hongge and Panzhihua magmatic Fe–Ti–V oxide deposits, Emeishan large igneous province, SW China. Economic Geology, 109, 1763–1785.

Bai, Z.-J., Zhong, H., Li, C., Zhu, W.-G., He, D.-F., and Hu, W.-J. (2016) Association of cumulus apatite with compositionally unusual olivine and plagioclase in the Taihe Fe-Ti oxide ore-bearing layered mafic-ultramafic intrusion: Petrogenetic significance and implications for ore genesis. American Minerlogist, 101, 2168–2175.

Barnes, S. (1986) The effect of trapped liquid crystallization on cumulus mineral compositions in layered intrusions. Contributions to Mineralogy and Petrology, 93, 524–531.

Barnes, S.J., Maier, W.D., and Ashwal, L.D. (2004) Platinum-group element distribution in the main zone and upper zone of the Bushveld Complex, South Africa. Chemical Geology, 208, 293–317.

Beattie, P. (1994) Systematics and energetics of trace-element partitioning between olivine and silicate melts: Implications for the nature of mineral/melt partitioning. Chemical Geology, 117, 57–71.

Cawthorn, R.G. (1996) Layered intrusions, 519 p. Elsevier Science.

—— (2007) Cr and Sr: Keys to parental magmas and processes in the Bushveld Complex, South Africa. Lithos, 95, 381–398.

—— (2013) Rare earth element abundances in apatite in the Bushveld Complex—A consequence of the trapped liquid shift effect. Geology, 41, 603–606.

650 Chen, L.-M., Song, X.-Y., Zhu, X.-K., Zhang, X.-Q., Yu, S.-Y., and Yi, J.-N. (2014)
651 Iron isotope fractionation during crystallization and sub-solidus re-equilibration:
652 Constraints from the Baima mafic layered intrusion, SW China. Chemical
653 Geology, 380, 97–109.
654 Chung, S.L., and Jahn, B.M. (1995) Plume-lithosphere interaction in generation of the
655 Emeishan flood basalts at the Permian-Triassic boundary. Geology, 23, 889–892.
656 Dare, S.A.S., Barnes, S.-J., and Beaudoin, G. (2012) Variation in trace element
657 content of magnetite crystallized from a fractionating sulfide liquid, Sudbury,
658 Canada: Implications for provenance discrimination. Geochimica et
659 Cosmochimica Acta, 88, 27–50.
660 Dare, S.A.S., Barnes, S.-J., Beaudoin, G., Méric, J., Boutroy, E., and Potvin-Doucet,
661 C. (2014) Trace elements in magnetite as petrogenetic indicators. Mineralium
662 Deposita 49, 785–796
663 Dygert, N., Liang, Y., and Hess, P. (2013) The importance of melt TiO_2 in affecting
664 major and trace element partitioning between Fe–Ti oxides and lunar picritic
665 glass melts. Geochimica et Cosmochimica Acta, 106, 134–151.
666 Dygert, N., Liang, Y., Sun, C., and Hess, P. (2014) An experimental study of trace
667 element partitioning between augite and Fe-rich basalts. Geochimica et
668 Cosmochimica Acta, 132, 170-186.
669 Eales, H.V., and Cawthorn, R.G. (1996). The Bushveld Complex. In R. G. Cawthorn,
670 Ed., Layered Intrusions, p. 181-229. Elsevier.
671 Egorova, V., and Latypov, R. (2013) Mafic–Ultramafic Sills: New Insights from M-

672 and S-shaped Mineral and Whole-rock Compositional Profiles. Journal of
673 Petrology, 54, 2155–2191.
674 Fenner, C.N. (1929) The crystallization of basalts. American Journal of Science, 18,
675 225–253.
676 Forien, M., Tremblay, J., Barnes, S.-J., Burgisser, A., and Pagé, P. (2015) The role of
677 viscous particle segregation in forming chromite layers from slumped crystal
678 slurries: Insights from analogue experiments. Journal of Petrology, 56, 2425–
679 2444.
680 Frost, B.R., and Lindsley, D.H. (1991) Occurrence of iron-titanium oxides in igneous
681 rocks. Reviews in Mineralogy and Geochemistry, 25, 433–468.
682 Ganino, C., Arndt, N.T., Zhou, M.F., Gaillard, F., and Chauvel, C. (2008) Interaction
683 of magma with sedimentary wall rock and magnetite ore genesis in the
684 Panzhihua mafic intrusion, SW China. Mineralium Deposita, 43, 677–694.
685 Ghiorso,M. S. and R. O. Sack (1995) Chemical mass transfer in magmatic processes.
686 IV. A revised and internally consistent thermodynamic model for the
687 interpolation and extrapolation of liquid-solid equilibria in magmatic systems at
688 elevated temperatures and pressures. Contributions to Mineralogy and Petrology,
689 119, 197–212.
690 Godel, B., Barnes, S.-J., and Maier, W.D. (2011) Parental magma composition
691 inferred from trace element in cumulus and intercumulus silicate minerals: An
692 example from the Lower and Lower Critical Zones of the Bushveld Complex,
693 South-Africa. Lithos, 125, 537–552.

694 Greig, J.W. (1927) Immiscibility in silicate melts. American Journal of Science, 13,
695 133–154.
696 Hart, S.R. and Dunn, T. (1993) Experimental cpx/melt partitioning of 24 trace
697 elements. Contributions to Mineralogy and Petrology, 113, 1–8.
698 Hauri, E.H., Wagner, T.P. and Grove, T.L. (1994) Experimental and natural
699 partitioning of Th, U, Pb and other trace elements between garnet, clinopyroxene
700 and basaltic melts. Chemical Geology, 117, 149–166.
701 Hou, T., Zhang, Z., Encarnacion, J., Santosh, M., and Sun, Y. (2013) The role of
702 recycled oceanic crust in magmatism and metallogeny: Os–Sr–Nd isotopes, U–
703 Pb geochronology and geochemistry of picritic dykes in the Panzhihua giant Fe–
704 Ti oxide deposit, central Emeishan large igneous province, SW China.
705 Contributions to Mineralogy and Petrology, 165, 805–822.
706 Howarth, G.H., and Prevec, S.A. (2013) Trace element, PGE, and Sr–Nd isotope
707 geochemistry of the Panzhihua mafic layered intrusion, SW China: Constraints
708 on ore-forming processes and evolution of parent magma at depth in a
709 plumbing-system. Geochimica et Cosmochimica Acta, 120, 459–478.
710 Howarth, G.H., Prevec, S.A., and Zhou, M.-F. (2013) Timing of Ti-magnetite
711 crystallisation and silicate disequilibrium in the Panzhihua mafic layered
712 intrusion: Implications for ore-forming processes. Lithos, 170–171, 73–89.
713 Jakobsen, J.K., Tegner, C., Brooks, C.K., Kent, A.J.R., Lesher, C.E., Nielsen, T.F.D.,
714 and Wiedenbeck, M. (2010) Parental magma of the Skaergaard intrusion:
715 constraints from melt inclusions in primitive troctolite blocks and FG-1 dykes.

716 Contributions to Mineralogy and Petrology, 159, 61–79.
717 Jang, Y.D., and Naslund, H.R. (2001) Major and trace element composition of
718 Skaergaard plagioclase; geochemical evidence for changes in magma dynamics
719 during the final stage of crystallization of the Skaergaard intrusion. Contributions
720 to Mineralogy and Petrology, 140, 441–457.
721 —— (2003) Major and trace element variation in ilmenite in the Skaergaard Intrusion:
722 petrologic implications. Chemical Geology, 193, 109–125.
723 Jourdan, F., Bertrand, H., Scharer, U., Blichert-Toft, J., Feraud, G., and Kampunzu,
724 A.B. (2007) Major and trace element and Sr, Nd, Hf and Pb isotope compositions
725 of the Karoo large igneous province, Botswana-Zimbabwe: Lithosphere vs
726 mantle plume contribution. Journal of Petrology, 48, 1043–1077.
727 Kamenetsky, V.S., Chung, S.L., Kamenetsky, M.B., and Kuzmin, D.V. (2012) Picrites
728 from the Emeishan Large Igneous Province, SW China: a Compositional
729 Continuum in Primitive Magmas and their Respective Mantle Sources. Journal
730 of Petrology, 53, 2095–2113.
731 Kloeck, W., and Palme, H. (1988) Partitioning of siderophile and chalcophile
732 elements between sulfide, olivine, and glass in a naturally reduced basalt from
733 Disko Island, Greenland. In G. Ryder, Ed., Proceedings of the Lunar and
734 Planetary Science Conference, 18, p. 471–483. Pergamon, New York.
735 Laubier, M., Grove, T.L., and Langmuir, C.H. (2014) Trace element mineral/melt
736 partitioning for basaltic and basaltic andesitic melts: An experimental and laser
737 ICP-MS study with application to the oxidation state of mantle source regions.

738 Earth and Planetary Science Letters, 392, 265–278.
739 Liu, P.-P., Zhou, M.-F., Chen, W.T., Boone, M., and Cnudde, V. (2014) Using
740 Multiphase Solid Inclusions to Constrain the Origin of the Baima Fe–Ti–(V)
741 Oxide Deposit, SW China. Journal of Petrology, 55, 951–976.
742 Liu, P.-P., Zhou, M.-F., Chen, W.T., Gao, J.-F., and Huang, X.-W. (2015) In-situ
743 LA-ICP-MS trace elemental analyses of magnetite: Fe–Ti–(V) oxide-bearing
744 mafic–ultramafic layered intrusions of the Emeishan Large Igneous Province,
745 SW China. Ore Geology Reviews, 65, 853–871.
746 Liu, Y., Hu, Z., Gao, S., Günther, D., Xu, J., Gao, C., and Chen, H. (2008) In situ
747 analysis of major and trace elements of anhydrous minerals by LA-ICP-MS
748 without applying an internal standard. Chemical Geology, 257, 34–43.
749 Luan, Y., Song, X.-Y., Chen, L.-M., Zheng, W.-Q., Zhang, X.-Q., Yu, S.-Y., She, Y.-W.,
750 Tian, X.-L., and Ran, Q.-Y. (2014) Key factors controlling the accumulation of
751 the Fe–Ti oxides in the Hongge layered intrusion in the Emeishan Large Igneous
752 Province, SW China. Ore Geology Reviews, 57, 518–538.
753 Lundgaard, K.L., Tegner, C., Cawthorn, R.G., Kruger, F.J., and Wilson, J.R. (2006)
754 Trapped intercumulus liquid in the Main Zone of the eastern Bushveld Complex,
755 South Africa. Contributions to Mineralogy and Petrology, 151, 352-369.
756 Maier, W.D., Barnes, S.J., and Groves, D.I. (2013) The Bushveld Complex, South
757 Africa: formation of platinum–palladium, chrome- and vanadium-rich layers via
758 hydrodynamic sorting of a mobilized cumulate slurry in a large, relatively slowly
759 cooling, subsiding magma chamber. Miner Deposita, 48, 1–56.

760 Namur, O., Charlier, B., Toplis, M.J., Higgins, M.D., Liegeois, J.P., and Vander
761 Auwera, J. (2010) Crystallization sequence and magma chamber processes in the
762 ferrobasaltic Sept Iles layered intrusion, Canada. Journal of Petrology, 51, 1203–
763 1236.
764 Pang, K.N., Li, C.S., Zhou, M.F., and Ripley, E.M. (2008a) Abundant Fe–Ti oxide
765 inclusions in olivine from the Panzhihua and Hongge layered intrusions, SW
766 China: evidence for early saturation of Fe–Ti oxides in ferrobasaltic magma.
767 Contributions to Mineralogy and Petrology, 156, 307–321.
768 Pang, K.N., Zhou, M.F., Lindsley, D., Zhao, D., and Malpas, J. (2008b) Origin of Fe–
769 Ti oxide ores in mafic intrusions: Evidence from the Panzhihua intrusion, SW
770 China. Journal of Petrology, 49, 295–313.
771 Pang, K.N., Li, C.S., Zhou, M.F., and Ripley, E.M. (2009) Mineral compositional
772 constraints on petrogenesis and oxide ore genesis of the late Permian Panzhihua
773 layered gabbroic intrusion, SW China. Lithos, 110, 199–214.
774 Panxi Geological Unit (1984) Mineralization and exploration forecasting of V–Ti
775 magnetite deposits in the Panzhihua–Xichang region. Unpublished (in Chinese).
776 Peach, C.L., Mathez, E.A., and Keays, R.R. (1990) Sulfide melt-silicate melt
777 distribution coefficients for noble metals and other chalcophile elements as
778 deduced from MORB: Implications for partial melting. Geochimica et
779 Cosmochimica Acta, 54, 3379–3389.
780 Pedersen, A.K. (1979). Basaltic glass with high-temperature equilibrated immiscible
781 sulfide bodies with native iron from disko, central west Greenland. Contributions

to Mineralogy and Petrology, 69, 397–407.

Philpotts, A.R. (1979) Silicate liquid immiscibility in tholeiitic basalts. Journal of Petrology, 20, 99–118.

Rajamani, V., and Naldrett, A.J. (1978) Partitioning of Fe, Co, Ni, and Cu between sulfide liquid and basaltic melts and the composition of Ni–Cu sulfide deposits. Economic Geology, 73, 82–93.

She, Y.-W., Yu, S.-Y., Song, X.-Y., Chen, L.-M., Zheng, W.-Q., and Luan, Y. (2014) The formation of P-rich Fe–Ti oxide ore layers in the Taihe layered intrusion, SW China: Implications for magma-plumbing system process. Ore Geology Reviews, 57, 539–559.

She, Y.-W., Song, X.-Y., Yu, S.-Y., and He, H.-L. (2015) Variations of trace element concentration of magnetite and ilmenite from the Taihe layered intrusion, Emeishan large igneous province, SW China: Implications for magmatic fractionation and origin of Fe–Ti–V oxide ore deposits. Journal of Asian Earth Sciences, 113, 1117–1131

Shellnutt, J.G., Denyszyn, S.W., and Mundil, R. (2012) Precise age determination of mafic and felsic intrusive rocks from the Permian Emeishan large igneous province (SW China). Gondwana Research, 22, 118–126.

Song, X.Y., Zhou, M.F., Hou, Z.Q., Cao, Z.M., Wang, Y.L., and Li, Y.G. (2001) Geochemical constraints on the mantle source of the upper permian Emeishan continental flood basalts, southwestern China. International Geology Review, 43, 213–225.

804 Song, X.Y., Zhou, M.F., Cao, Z.M., and Robinson, P.T. (2004) Late permian rifting of
805 the South China Craton caused by the Emeishan mantle plume? Journal of the
806 Geological Society, 161, 773–781.
807 Song, X.Y., Qi, H.W., Robinson, P.T., Zhou, M.F., Cao, Z.M., and Chen, L.M. (2008)
808 Melting of the subcontinental lithospheric mantle by the Emeishan mantle plume;
809 evidence from the basal alkaline basalts in Dongchuan, Yunnan, Southwestern
810 China. Lithos, 100, 93–111.
811 Song, X.Y., Qi, H.W., Hu, R.Z., Chen, L.M., Yu, S.Y., and Zhang, J.F. (2013)
812 Formation of thick stratiform Fe–Ti oxide layers in layered intrusion and
813 frequent replenishment of fractionated mafic magma: Evidence from the
814 Panzhihua intrusion, SW China. Geochemistry Geophysics Geosystems, 14,
815 712–732.
816 Tanner, D., Mavrogenes, J.A., Arculus, R.J., and Jenner, F.E. (2014) Trace Element
817 Stratigraphy of the Bellevue Core, Northern Bushveld: Multiple Magma
818 Injections Obscured by Diffusive Processes. Journal of Petrology, 55, 859–882.
819 Thy P, Lesher C E, Nielsen T F D, Brooks C K. (2006) Experimental constraints on
820 the Skaergaard liquid line of descent. Lithos, 92, 154–180.
821 Toplis, M.J., and Carroll, M.R. (1995) An experimental study of the influence of
822 oxygen fugacity on Fe–Ti oxide stability, phase relations, and mineral-melt
823 equilibria in ferro-basaltic systems. Journal of Petrology, 36, 1137–1170.
824 Tribuzio, R., Tiepolo, M., Vannucci, R., and Bottazzi, P. (1999) Trace element
825 distribution within olivine-bearing gabbros from the Northern Apennine

826 ophiolites (Italy): evidence for post-cumulus crystallization in MOR-type
827 gabbroic rocks. Contributions to Mineralogy and Petrology, 134, 123–133.
828 van Kan Parker, M., Mason, P.R.D., and van Westrenen, W. (2011) Trace element
829 partitioning between ilmenite, armalcolite and anhydrous silicate melt:
830 Implications for the formation of lunar high-Ti mare basalts. Geochimica et
831 Cosmochimica Acta, 75, 4179–4193.
832 Vantongeren, J.A., and Mathez, E.A. (2013) Incoming Magma Composition and Style
833 of Recharge below the Pyroxenite Marker, Eastern Bushveld Complex, South
834 Africa. Journal of Petrology, 54, 1585–1605.
835 Wager, L.R., and Brown, G.M. (1967) Layered igneous rocks. Oliver and Boyd,
836 Edinburgh.
837 Xing, C.M., Wang, C.Y., and Li, C.Y. (2014) Trace element compositions of apatite
838 from the middle zone of the Panzhihua layered intrusion, SW China: Insights
839 into the differentiation of a P- and Si-rich melt. Lithos, 204, 188–202.
840 Xu, Y.G., Chung, S.L., Jahn, B.M., and Wu, G.Y. (2001) Petrologic and geochemical
841 constraints on the petrogenesis of Permian-Triassic Emeishan flood basalts in
842 southwestern China. Lithos, 58, 145–168.
843 Xu, Y.G., He, B., Chung, S.L., Menzies, M.A., and Frey, F.A. (2004) Geologic,
844 geochemical, and geophysical consequences of plume involvement in the
845 Emeishan flood-basalt province. Geology, 32, 917–920.
846 Zhang, Y.-X., Luo, Y.-N., and Yang, C.-X. (1988) The Panxi Rift, Geological Press,
847 Beijing (in Chinese).

Zhang, X.-Q., Zhang, J.-F., Yuan, P., Song, X.-Y., Guan, J.-X., and Deng, Y.-F. (2011) Implications of compositions of plagioclase and olivine on the formation of the Panzhihua V–Ti magnetite deposit, Sichuan Province. Acta Petrologica Sinica, 27, 3675–3688 (in Chinese with English abstract).

Zhang, X.-Q., Song, X.-Y., Chen, L.-M., Xie, W., Yu, S.-Y., Zheng, W.-Q., Deng, Y.-F., Zhang, J.-F., and Gui, S.-G. (2012) Fractional crystallization and the formation of thick Fe–Ti–V oxide layers in the Baima layered intrusion, SW China. Ore Geology Reviews, 49, 96–108.

Zhang, Z.C., Mahoney, J.J., Mao, J.W., and Wang, F.H. (2006) Geochemistry of picritic and associated basalt flows of the western Emeishan flood basalt province, China. Journal of Petrology, 47, 1997–2019.

Zhang, Z.C., Li, Y., Zhao, L., and Ai, Y. (2007) Geochemistry of three layered mafic-ultramafic intrusions in the Panxi area and constraints on their sources. Acta Petrologica Sinica, 23, 2339–2352.

Zheng, W.-Q., Deng, Y.-F., Song, X.-Y., Chen, L.-M., Yu, S.-Y., Zhou, G.-F., Liu, S.-R., and Xiang, J.-X. (2014) Composition and genetic significance of the ilmenite of the Panzhihua intrusion. Acta Petrologica Sinica, 30, 1432–1442.

Zhong, H., and Zhu, W.-G. (2006) Geochronology of layered mafic intrusions from the Pan–Xi area in the Emeishan large igneous province, SW China. Mineralium Deposita, 41, 599–606.

Zhong, H., Qi, L., Hu, R.-Z., Zhou, M.-F., Gou, T.-Z., Zhu, W.-G., Liu, B.-G., and Chu, Z.-Y. (2011) Rhenium-osmium isotope and platinum-group elements in the

Xinjie layered intrusion, SW China: Implications for source mantle composition, mantle evolution, PGE fractionation and mineralization. Geochimica et Cosmochimica Acta, 75, 1621–1641.

Zhou, M.-F., Yan, D.-P., Kennedy, A.K., Li, Y., and Ding, J. (2002) SHRIMP U–Pb zircon geochronological and geochemical evidence for Neoproterozoic arc-magmatism along the western margin of the Yangtze Block, South China. Earth and Planetary Science Letters, 196, 51–67.

Zhou, M.F., Robinson, P.T., Lesher, C.M., Keays, R.R., Zhang, C.J., and Malpas, J. (2005) Geochemistry, petrogenesis and metallogenesis of the Panzhihua gabbroic layered intrusion and associated Fe–Ti–V oxide deposits, Sichuan Province, SW China. Journal of Petrology, 46, 2253–2280.

Zhou, M.F., Arndt, N.T., Malpas, J., Wang, C.Y., and Kennedy, A.K. (2008) Two magma series and associated ore deposit types in the Permian Emeishan large igneous province, SW China. Lithos, 103, 352–368.

FIGURE CAPTIONS

Figure 1. (a) Major tectonic units of China (after Song et al. 2008). (b) Regional geological map of the Emeishan large igneous province, showing the distribution of the Emeishan continental flood basalts and location of the Panzhihua layered intrusion (modified after Song et al. 2001, 2008). (c) Geological map of the Panzhihua intrusion (modified after Panxi Geological Unit 1984 and Song et al. 2001, 2008).

Figure 2. Structures and microtextures of the Panzhihua rocks. (a) Massive Fe-Ti

892 oxide layers overlain by magnetite gabbro interlayers. (b) Polygonal magnetite and
893 ilmenite with straight to slightly curved boundaries and (occasionally) 120° triple
894 junctions in massive Fe-Ti oxide ores. Tiny primary sulfides (mainly pyrrhotite and
895 chalcopyrite) were included in Fe-Ti oxides. (c) Magnetite gabbro (Lower Zone) with
896 a bent plagioclase crystal rimmed by anhedral hornblende. (d) Two sets of exsolution
897 magnetite lamellae in clinopyroxene (parallel to prismatic cleavage in clinopyroxene)
898 with an overgrowth rim and anhedral hornblende rims (Lower Zone). (e) Magnetite
899 gabbro (Middle Zone) with regular and linear boundaries between clinopyroxene and
900 plagioclase with rare hornblende rims. (f) Apatite gabbro (Upper Zone) with
901 fine-grained euhedral apatite inclusions in clinopyroxene and plagioclase, and
902 disseminated Fe-Ti oxides among silicates. Cpx: clinopyroxene; Pl: plagioclase; Mt:
903 magnetite; Ilm: ilmenite; Ap: apatite; Oxide: magnetite and ilmenite.

904 **Figure 3.** Comparison of LA-ICP-MS analytical results for (a) In-house magnetite
905 standard (BC-28; from the Bushveld Complex) and (b) International reference
906 materials (KL2-G and ML3B-G) with their preferred values. The preferred values of
907 BC-28 are from Barnes et al. (2004) and Dare et al. (2012, 2014) and those of KL2-G
908 and ML3B-G are from the "GeoREM database" (http://georem.mpch-mainz.gwdg.de/
909 sample_query_pref.asp).

910 **Figure 4.** Variations of key trace elements and MgO (or $Mg^{\#}$) in magnetite, ilmenite,
911 and clinopyroxene with relative stratigraphic position of the Panzhihua intrusion.
912 Filled symbols are average contents of the trace element, error bars represent the
913 range measured in this study, and bright blue crosses are the mineral grains in contact

914 with anhedral hornblende rims.

915 **Figure 5.** Emeishan high-Ti picrite normalized multi-element diagrams for Panzhihua
916 magnetite (in increasing order of trace element compatibility with magnetite, after
917 Dare et al. 2012, 2014). Magmatic magnetite from the Bushveld Complex (light
918 yellow field, data from Dare et al. 2014) is plotted for comparison. The Emeishan
919 high-Ti picrite data are from Kamenetsky et al. (2012).

920 **Figure 6.** Emeishan high-Ti picrite normalized multi-element diagrams for Panzhihua
921 ilmenite (in increasing order of trace element compatibility with ilmenite, after Jang
922 and Naslund 2003; van Kan Parker et al. 2011; Dygert 2013). The Emeishan high-Ti
923 picrite data are from Kamenetsky et al. (2012).

924 **Figure 7.** Multi-element variation diagrams for Panzhihua clinopyroxene, normalized
925 to the average composition of clinopyroxene phenocrysts in the Emeishan high-Ti
926 picrite (clinopyroxene data are from Kamenetsky et al. 2012).

927 **Figure 8.** Correlation plots for the average contents of (a) Ni in clinopyroxene vs. Ni
928 in magnetite and ilmenite (y-axis on the left for magnetite; y-axis on the right for
929 ilmenite); (b) Cr in clinopyroxene vs. Cr in magnetite and ilmenite; (c) V in
930 clinopyroxene vs. V in magnetite and ilmenite; (d) Sc in clinopyroxene vs. Sc in
931 magnetite and ilmenite; and (e) Zr in clinopyroxene vs. Zr in magnetite and ilmenite
932 for the different Panzhihua rock types. Abbreviations: Cpx: Clinopyroxene, Mt:
933 Magnetite, Ilm: Ilmenite; DL: Detection Limit.

934 **Figure 9.** Binary plots for the average contents of (a) Cr in magnetite vs. Ni in

ilmenite, and (b) V in magnetite vs. V in ilmenite for the different Panzhihua rock types. Abbreviations: Mt: Magnetite, Ilm: Ilmenite; DL: Detection Limit.

APPENDICES

Table S1 Comparisons of reference standards between LA-ICP-MS results in this study and their preferred values

Table S2. LA-ICP-MS results of major and trace elements (ppm) in the Panzhihua magnetite

Table S3. LA-ICP-MS results of major and trace elements (ppm) in the Panzhihua ilmenite

Table S4. LA-ICP-MS results of major and trace elements (ppm) in the Panzhihua clinopyroxene

Table S5. A summary of mineral/silicate liquid partition coefficients of selected elements

This is a preprint, the final version is subject to change, of the American Mineralogist (MSA)
Cite as Authors (Year) Title. American Mineralogist, in press.
(DOI will not work until issue is live.) DOI: http://dx.doi.org/10.2138/am-2017-5804

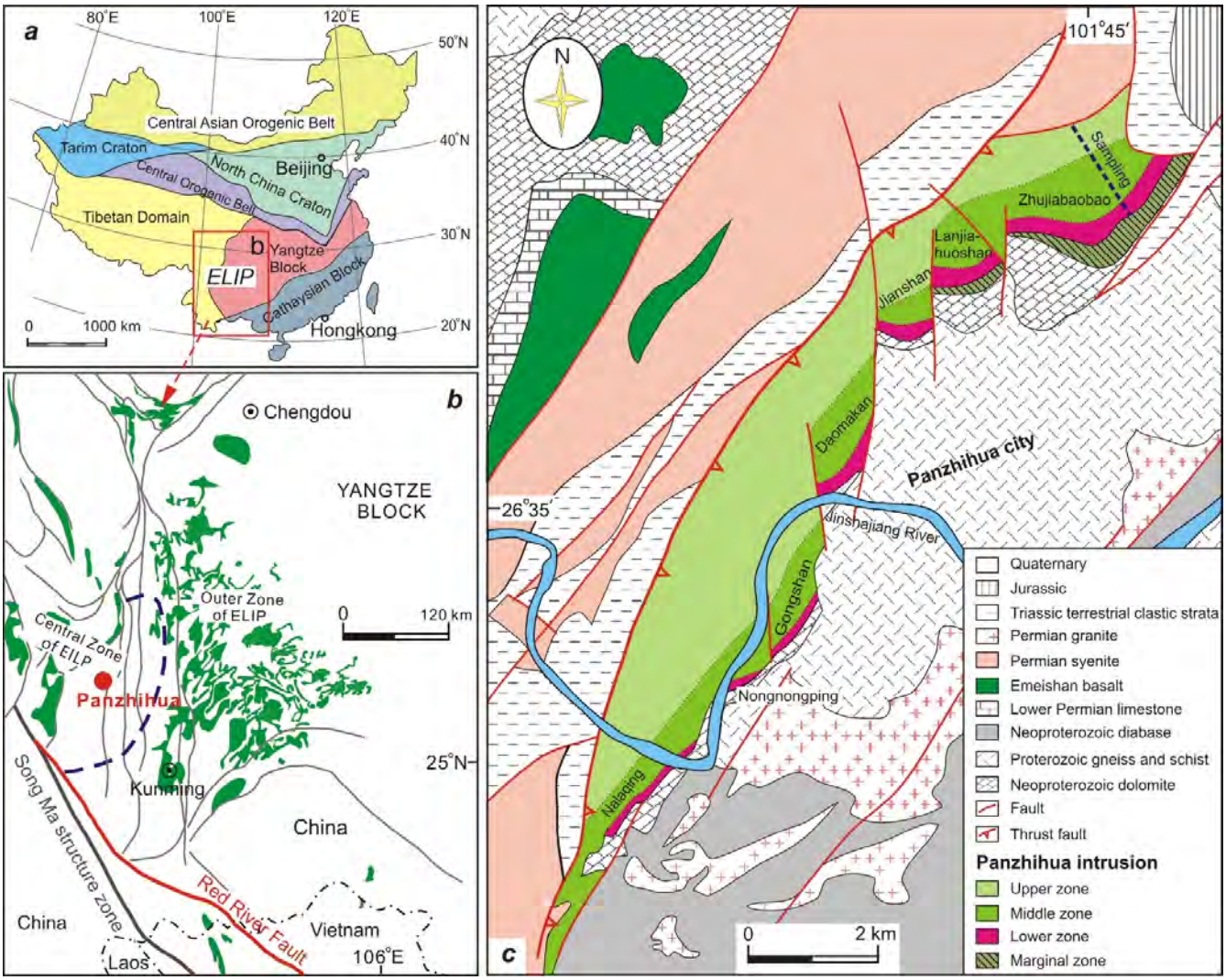

Fig. 1

This is a preprint, the final version is subject to change, of the American Mineralogist (MSA)
Cite as Authors (Year) Title. American Mineralogist, in press.
(DOI will not work until issue is live.) DOI: http://dx.doi.org/10.2138/am-2017-5804

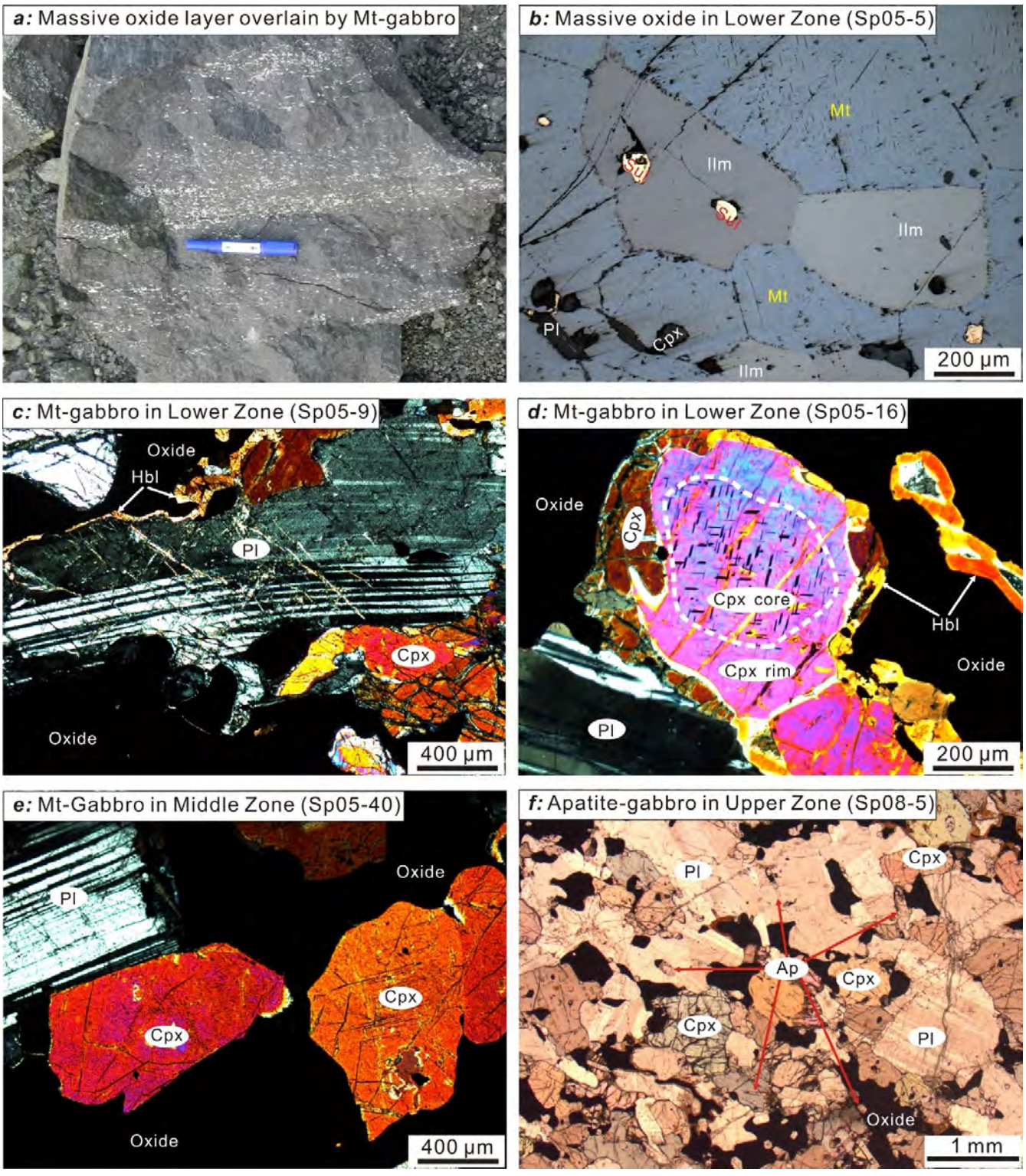

Fig. 2

This is a preprint, the final version is subject to change, of the American Mineralogist (MSA)
Cite as Authors (Year) Title. American Mineralogist, in press.
(DOI will not work until issue is live.) DOI: http://dx.doi.org/10.2138/am-2017-5804

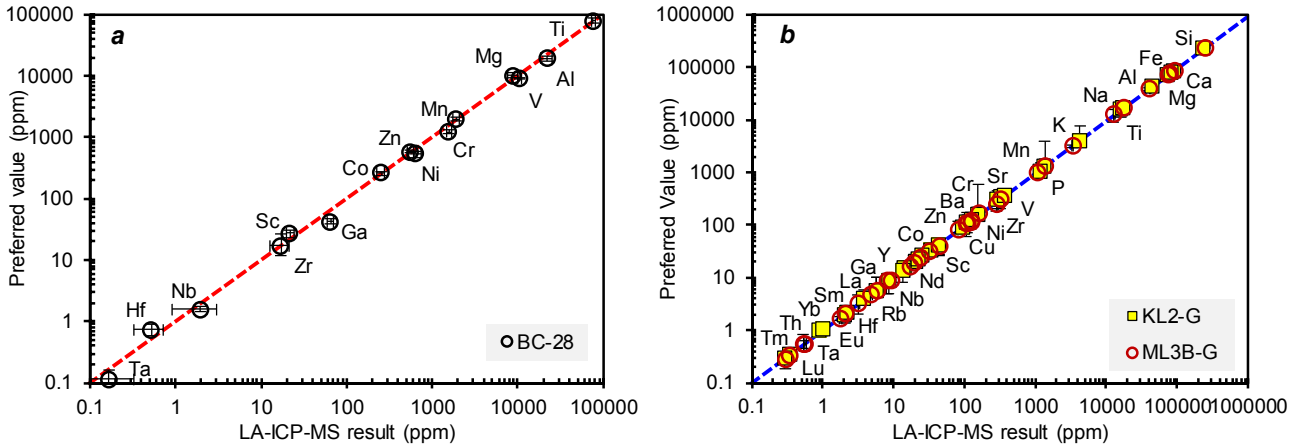

Fig. 3

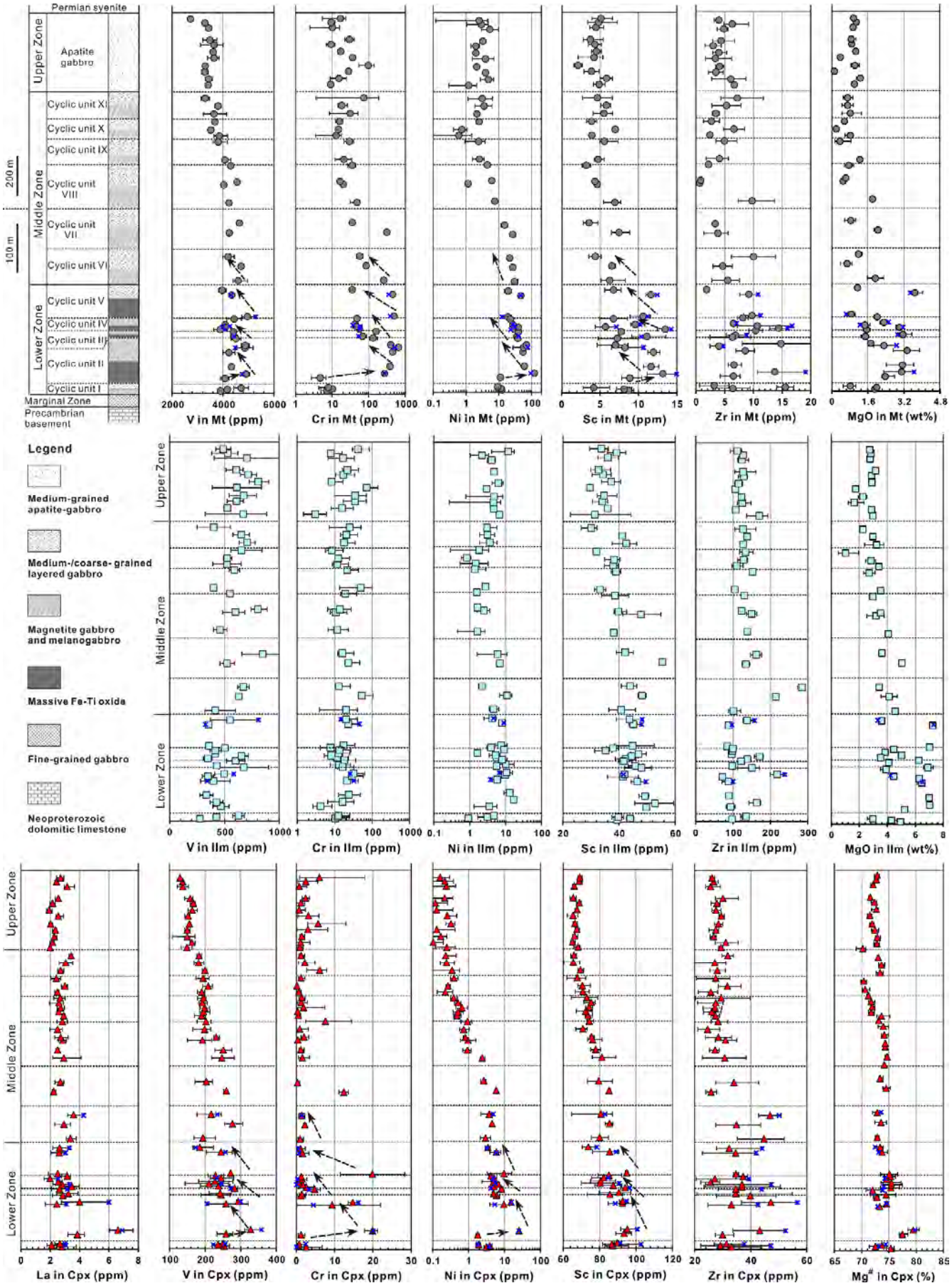
Permian syenite
Upper Zone
Apatite gabbro
Middle Zone
Cyclic unit XI
Cyclic unit X
Cyclic unit IX
Cyclic unit VIII
Cyclic unit VII
Cyclic unit VI
Lower Zone
Cyclic unit V
Cyclic unit IV
Cyclic unit III
Cyclic unit II
Cyclic unit I
Marginal Zone
Precambrian basement
200 m
100 m
V in Mt (ppm)
Cr in Mt (ppm)
Ni in Mt (ppm)
Sc in Mt (ppm)
Zr in Mt (ppm)
MgO in Mt (wt%)
Legend
Medium-grained apatite-gabbro
Medium-/coarse- grained layered gabbro
Magnetite gabbro and melanogabbro
Massive Fe-Ti oxide
Fine-grained gabbro
Neoproterozoic dolomitic limestone
V in Ilm (ppm)
Cr in Ilm (ppm)
Ni in Ilm (ppm)
Sc in Ilm (ppm)
Zr in Ilm (ppm)
MgO in Ilm (wt%)
La in Cpx (ppm)
V in Cpx (ppm)
Cr in Cpx (ppm)
Ni in Cpx (ppm)
Sc in Cpx (ppm)
Zr in Cpx (ppm)
Mg# in Cpx (%)

Fig. 4

This is a preprint, the final version is subject to change, of the American Mineralogist (MSA)
Cite as Authors (Year) Title. American Mineralogist, in press.
(DOI will not work until issue is live.) DOI: http://dx.doi.org/10.2138/am-2017-5804

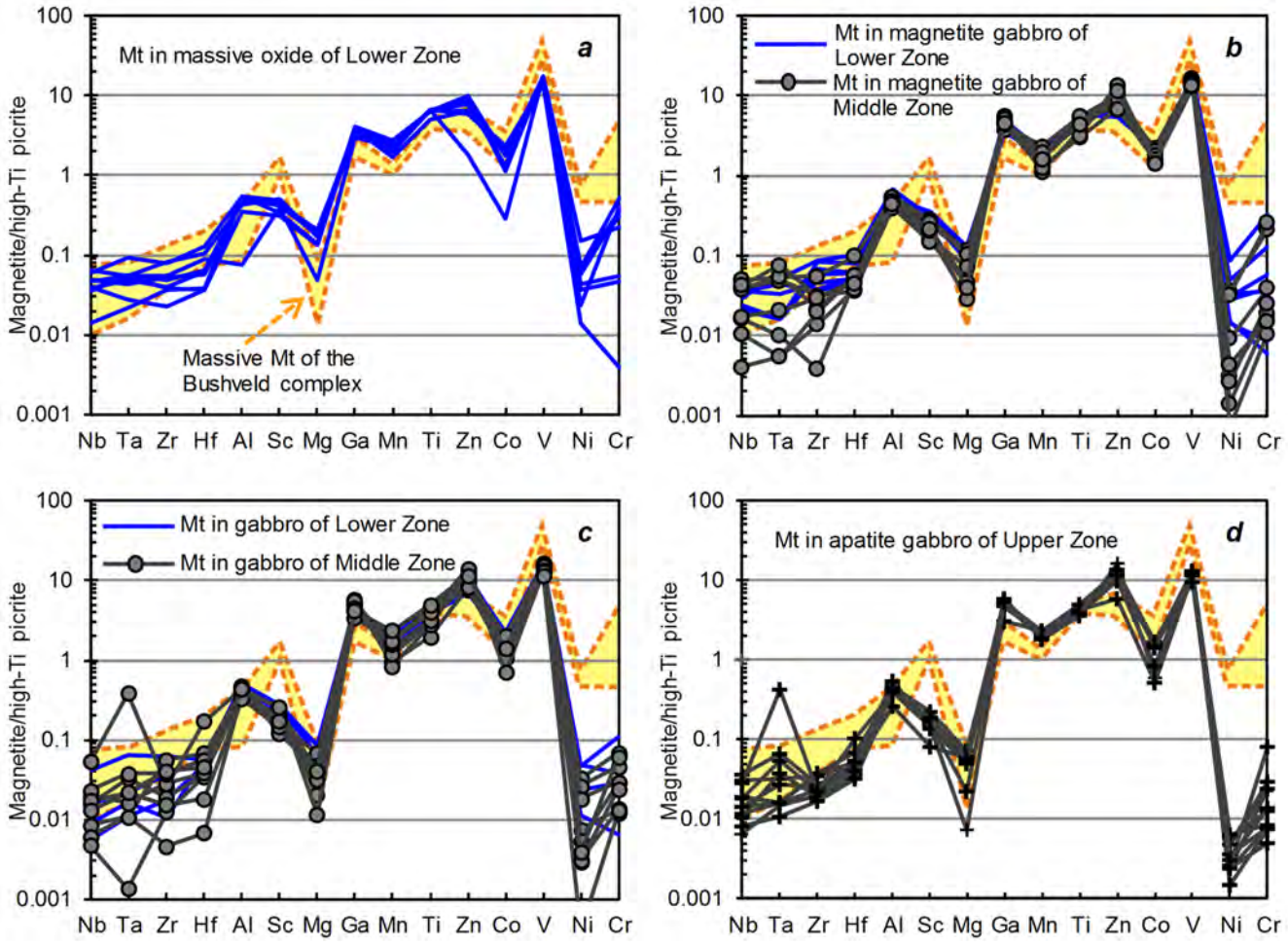

Fig. 5

This is a preprint, the final version is subject to change, of the American Mineralogist (MSA)
Cite as Authors (Year) Title. American Mineralogist, in press.
(DOI will not work until issue is live.) DOI: http://dx.doi.org/10.2138/am-2017-5804

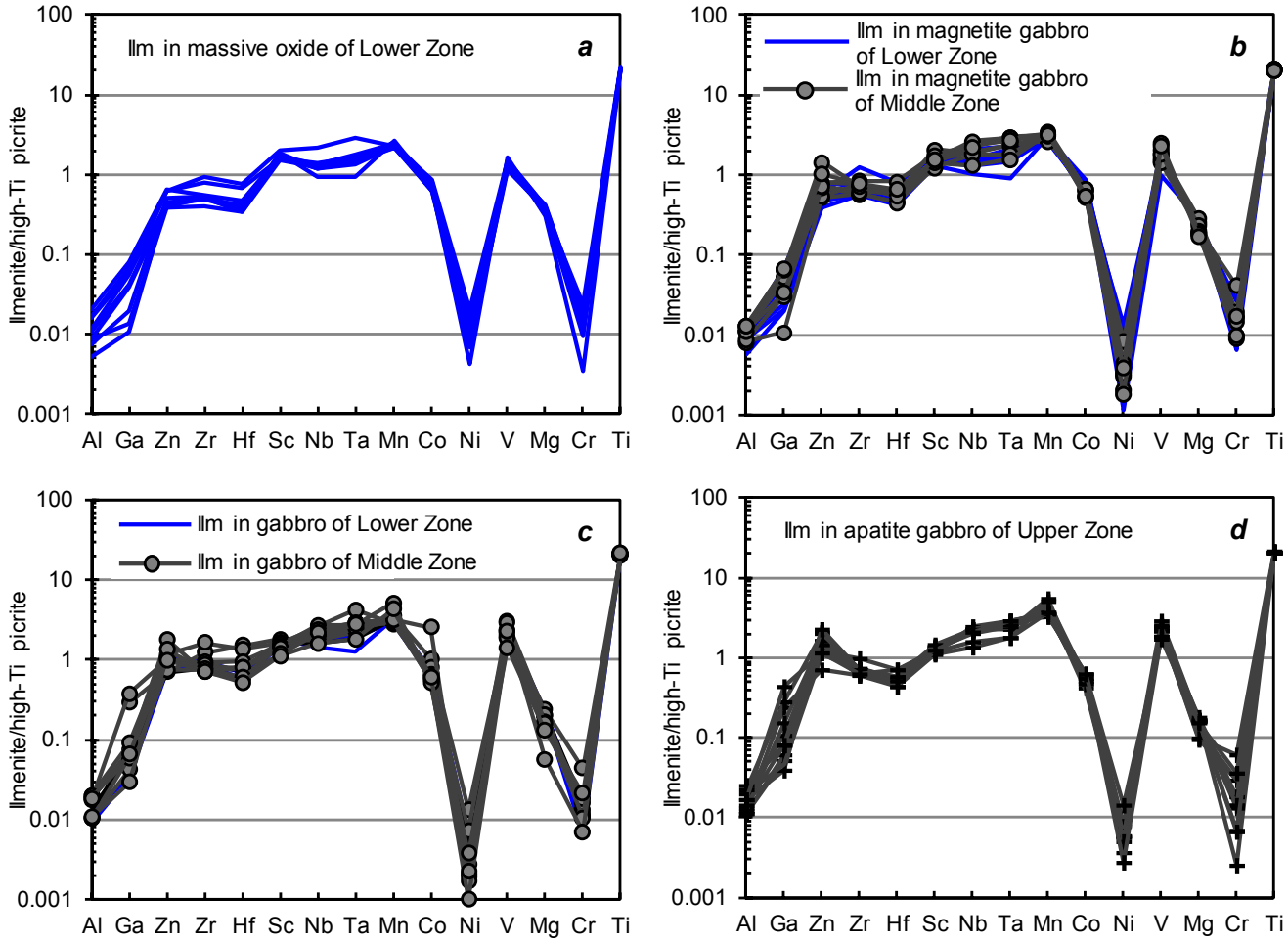

Fig. 6

This is a preprint, the final version is subject to change, of the American Mineralogist (MSA)
Cite as Authors (Year) Title. American Mineralogist, in press.
(DOI will not work until issue is live.) DOI: http://dx.doi.org/10.2138/am-2017-5804

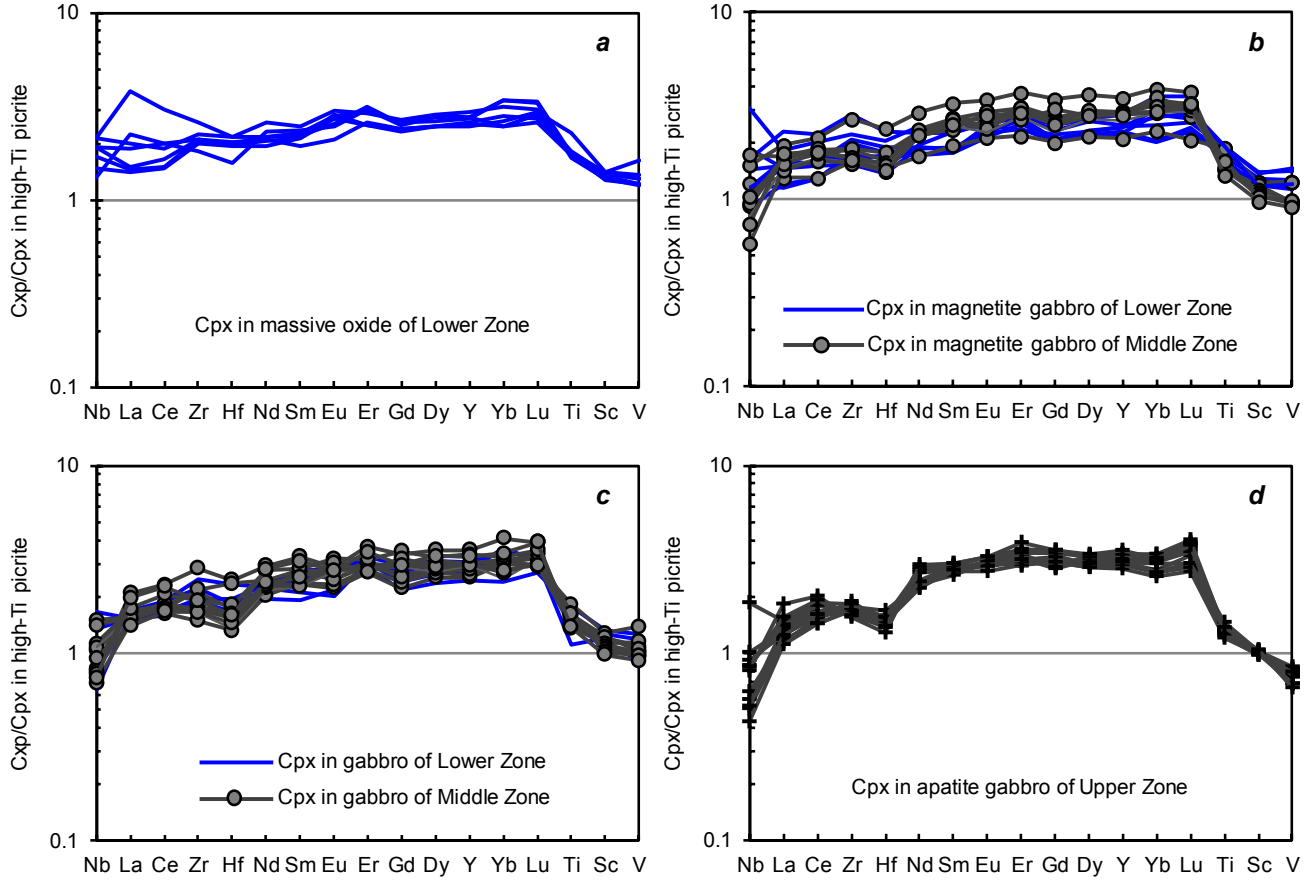

Fig. 7

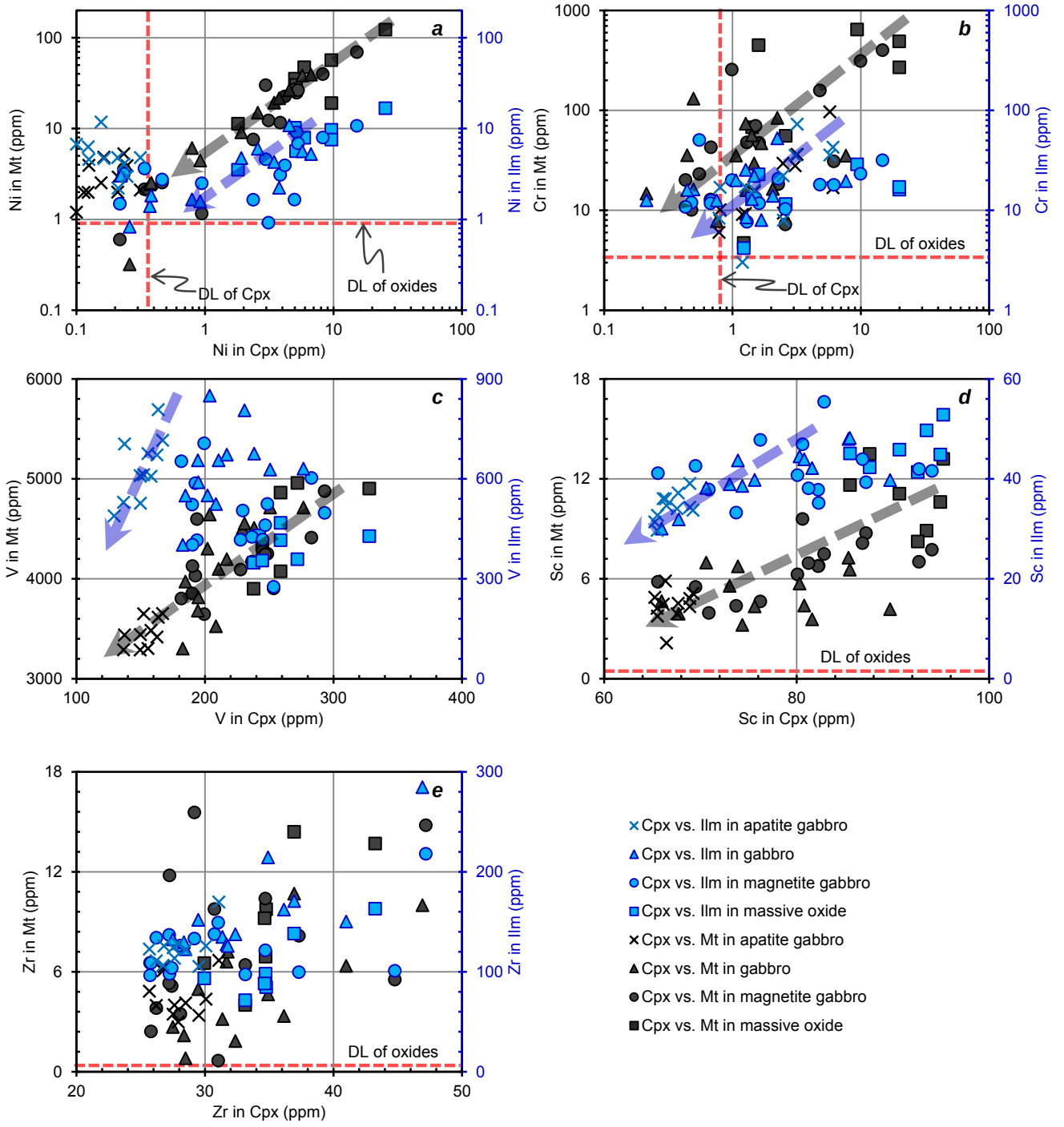
a
Ni in Mt (ppm)
Ni in Ilm (ppm)
Ni in Cpx (ppm)
DL of Cpx
DL of oxides
b
Cr in Mt (ppm)
Cr in Ilm (ppm)
Cr in Cpx (ppm)
DL of oxides
DL of Cpx
c
V in Mt (ppm)
V in Ilm (ppm)
V in Cpx (ppm)
d
Sc in Mt (ppm)
Sc in Ilm (ppm)
Sc in Cpx (ppm)
DL of oxides
e
Zr in Mt (ppm)
Zr in Ilm (ppm)
Zr in Cpx (ppm)
DL of oxides
Cpx vs. Ilm in apatite gabbro
Cpx vs. Ilm in gabbro
Cpx vs. Ilm in magnetite gabbro
Cpx vs. Ilm in massive oxide
Cpx vs. Mt in apatite gabbro
Cpx vs. Mt in gabbro
Cpx vs. Mt in magnetite gabbro
Cpx vs. Mt in massive oxide

Fig. 8

This is a preprint, the final version is subject to change, of the American Mineralogist (MSA)
Cite as Authors (Year) Title. American Mineralogist, in press.
(DOI will not work until issue is live.) DOI: http://dx.doi.org/10.2138/am-2017-5804

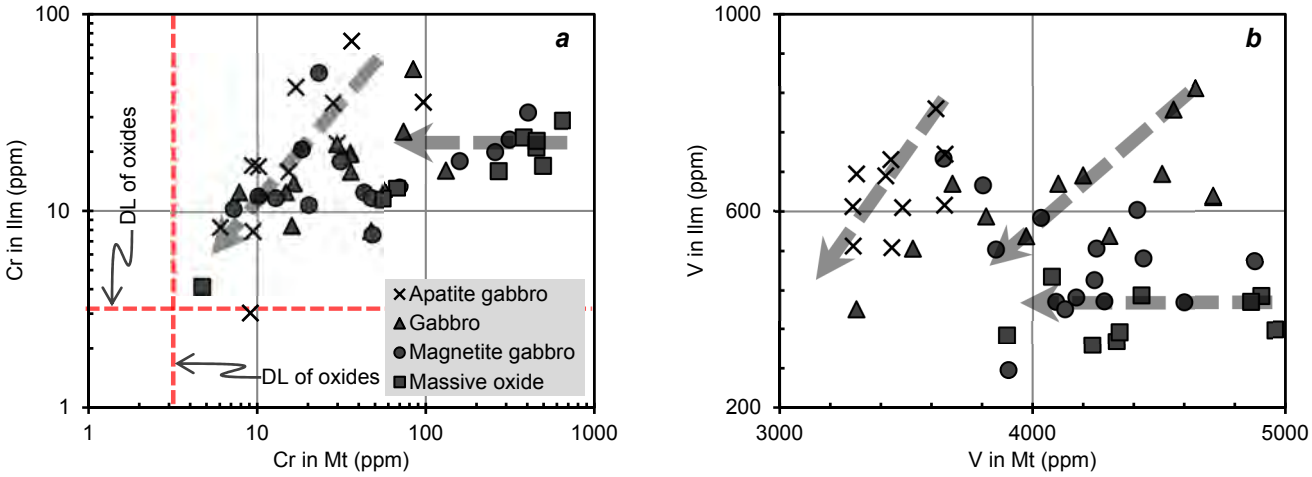

Fig. 9

This is a preprint, the final version is subject to change, of the American Mineralogist (MSA)
Cite as Authors (Year) Title. American Mineralogist, in press.
(DOI will not work until issue is live.) DOI: http://dx.doi.org/10.2138/am-2017-5804

Table 1 Magmatic stratigraphy of the Panzhihua layered intrusion, the Emeishan large igneous province

Characterization	Remarkable features	References
Upper Zone		
Defined by the abrupt appearance of cumulus apatite. The Upper Zone is dominated by apatite gabbro, which is made up of plagioclase (An = 23.5 – 53.3%), clinopyroxene ($Mg^{\#}$ = 51.3 – 74.8%), magnetite, ilmenite, and minor olivine (Fo = 27.7 – 64.5%) and apatite.	Free of Fe-Ti oxide ores. Low magnetite/ilmenite ratios.	Panxi Geological Unit 1984; Pang et al. 2009; Song et al. 2013; This study
Middle Zone		
Marked by magnetite gabbros without massive Fe-Ti oxide layers at base, overlain by gabbros. The mineral assemblages are similar to the Lower Zone, but are high proportions of plagioclase (An = 51.8 – 69.7%), clinopyroxene ($Mg^{\#}$ = 70.4 – 78.6%), and low abundances of magnetite, ilmenite, olivine (Fo = 65.4 – 82.3%) and hornblende without sulfides.	Some magnetite gabbro horizons are mined for Fe and Ti. Moderate magnetite/ilmenite ratios.	Panxi Geological Unit 1984; Zhou et al. 2005; Pang et al. 2009; Song et al. 2013; Zhang et al. 2011; This study
Lower Zone		
Marked by massive Fe-Ti oxide layers. The Lower Zone consists of Fe-Ti oxide layers, magnetite gabbros and gabrros, containing magnetite, ilmenite, plagioclase (An = 57.5 – 62.5%), clinopyroxene ($Mg^{\#}$ = 72.0 – 79.2%), and minor olivine (Fo = 64.4 – 80.7%), hornblende and sulfides.	Several thick stratiform Fe-Ti oxide layers and magnetite gabbros horizons are mined for Fe, Ti, and V. High magnetite/ilmenite ratios.	Panxi Geological Unit 1984; Zhou et al. 2005; Pang et al. 2009; Song et al. 2013; Zhang et al. 2011; This study
Marginal Zone		
The Marginal Zone is composed of micrograbbroic rocks and is proposed to be the chilled base of the intrusion. The mineral assemblages are fine-grained plagioclase (An = 49.6 – 72.1%), clinopyroxene ($Mg^{\#}$ = 80.3 – 84.6%), hornblende, magnetite, ilmenite, and minor olivine (Fo = 77.9 – 81.1%) and apatite.	No economic horizons of Fe, Ti, and V. Fine-grained texture of minerals.	Zhou et al. 2005; Pang et al. 2009